J. Fluid Mech. (1982), *vol.* 122, *pp.* 13–56
Printed in Great Britain

The structure of turbulent boundary layers at low Reynolds numbers

By J. MURLIS,† H. M. TSAI AND P. BRADSHAW
Department of Aeronautics, Imperial College, London SW7 2BY

(Received 7 July 1980 and in revised form 26 August 1981)

Conditionally sampled hot-wire and 'cold-wire' (resistance-thermometer) measurements confirm the general flow picture advanced by Falco (1974, 1977, 1980; see also Smith & Abbott 1978) and by Head & Bandyopadhyay (1981; see also Smith & Abbott) on the basis of smoke observations and more limited hot-wire measurements. The probability density function of turbulent-zone lengths in the intermittent region varies rapidly with Reynolds number, supporting the above authors' finding that the hairpin-vortex 'typical eddies' in the viscous superlayer scale on the viscous length ν/u_τ rather than on boundary-layer thickness. However the average turbulent-zone length, deduced as an integral moment of the probability distribution, tends to a constant fraction of the boundary-layer thickness above a momentum-thickness Reynolds number of 5000, which strongly suggests that at high Reynolds numbers the overall shape of the turbulent irrotational interface is controlled by the classical 'large eddies' and not by the viscosity-dependent small eddies. The intermittency profile is practically independent of Reynolds number. The second-order structural parameter $\overline{u^2}/\overline{v^2}$ increases strongly with increasing Reynolds number but the triple-product parameters, with the exception of the u-component skewness, vary only slowly with Reynolds number. This behaviour of the intermittency and velocity statistics is most simply explained by supposing that the lengthscale of the large eddies is nearly independent of Reynolds number while their intensity is somewhat lower at low Reynolds number. 'Typical eddies' evidently contribute to the Reynolds stresses at low Reynolds number, but it is probable that the large eddies carry most of the triple products at any Reynolds number. Our results confirm the usual finding that the mixing length and dissipation length parameter increase, while the wake component of the velocity profile decreases, as Reynolds number decreases.

1. Introduction

The usual analysis for the velocity defect in a turbulent boundary layer in zero pressure gradient, given for instance by Townsend (1956), leads to the expression

$$\frac{U_e - U}{U_\tau} = f\left(\frac{y}{\delta}\right) \tag{1}$$

where $u_\tau = (\tau_w/\rho)^{\frac{1}{2}}$ is the friction velocity. The analysis assumes that the direct effect of the parameter $u_\tau/U_e = (\frac{1}{2}c_f)^{\frac{1}{2}}$ or equivalently $d\tau_w/dx$, is negligible. It is possible that the effect of c_f is responsible for the slight Reynolds-number dependence of (1) at high Reynolds number, especially in supersonic flow, discussed by Mabey (1977, see also Mabey 1979). However, Coles (1962) found comparatively large changes in turbulent

† Present address: Centre for Overseas Pest Research, Wright's Lane, London W8.

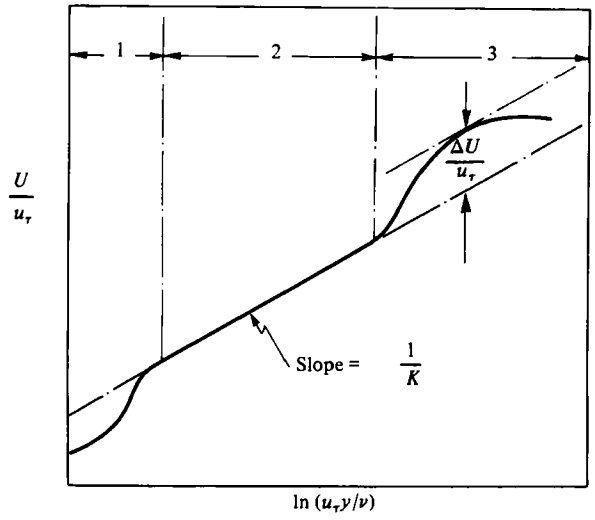

FIGURE 1. Definition sketch of mean-velocity profile. Region 1: viscous sublayer, $u_\tau y/\nu < 30$ approx. Region 2: logarithmic layer, $y/\delta < 0{\cdot}2$ approx. Region 3: outer layer: $\Delta U/u_\tau \equiv 2\Pi/\kappa$, where Π is wake parameter. At $Re_\theta = 2000$, $u_\tau\delta/\nu \approx 800$.

boundary layers in zero pressure gradient at momentum-thickness Reynolds numbers $u_e\theta/\nu$ of less than about 5000, and it has generally been assumed that this is a direct effect of Reynolds number itself rather than an effect of c_f; that is, it is an effect of viscosity on the turbulence structure outside the viscous sublayer (the defect-law analysis assumes viscous effects to be confined to the sublayer $u_\tau y/\nu < 30$, say; see figure 1). Huffman & Bradshaw (1972) showed that the velocity-defect profile in pipe flow is apparently independent of Reynolds number, even in the low-Reynolds-number range, and the simplest hypothesis to explain this difference between boundary-layer and pipe flow is to suppose that the Reynolds-number effects on the defect law are associated with the 'viscous *super*layer', that is, the region at the instantaneous edge of the turbulent boundary layer in which vorticity is transferred to originally irrotational fluid by the action of viscosity: in fully-developed pipe flow there is no such region. The thickness δ_{sup} of the viscous superlayer, like that δ_{sub} of the viscous sublayer, is likely to be some small multiple of the local value of the Kolmogorov thickness $\eta \equiv (\nu^3/\epsilon)^{\frac{1}{4}}$, where ϵ is the dissipation rate. At the edge of the viscous sublayer, η is about $\frac{1}{16}$ of δ_{sub}. Since ϵ is smaller, and η therefore larger, near the outer edge of the flow, this implies that the viscous superlayer is likely to be at least as thick as the viscous sublayer, and $\delta_{sub} \approx 0{\cdot}1\delta$ at the lowest Reynolds number at which turbulent flow can be maintained ($Re_\theta \approx 320$ according to Preston 1958). Furthermore the viscous superlayer covers the highly irregular interface between turbulent and non-turbulent flow, and so the total volume of fluid occupied by the viscous superlayer is many times larger than the thickness of the superlayer multiplied by its projected surface area. Paizis & Schwartz (1974) show that the ratio is at least 7, and their technique appears to ignore most of the small-scale corrugations. It is therefore highly probable that at low Reynolds numbers a large fraction of the outer-layer fluid in the boundary layer is in fact occupied by the viscous superlayer, and this clearly provides opportunities for significant viscous effects on the energy-containing motion.

The measurement of statistics of the interface position and of the 'intermittency function' γ is the earliest known application of the technique of conditional sampling

(Corrsin & Kistler 1955). More recently, the technique has been used for general studies of eddy structure: useful entries to the literature are provided by the conference proceedings edited by Fiedler (1978), Smith & Abbott (1978) and Kline & Falco (1980). It appears that the key to understanding low-Reynolds-number effects is the behaviour of the viscous superlayer, and that the key to measuring the behaviour of the viscous superlayer is conditional sampling; the work to be described below is based on this technique. Briefly, the 'conditional' average of a function $f(t)$, say the electrical output signal of a hot-wire probe, is the conventional (Reynolds) time average of $f(t)\,c(t)$, where the 'conditioning function' $c(t)$ is set equal to unity during times when $f(t)$ is 'interesting' according to some criterion chosen by the user; at other times $c(t)$ is set equal to zero. In intermittency studies $c(t) = 1$ when the flow at the point where $f(t)$ is measured is turbulent, and zero when the flow at that point is non-turbulent. Below, we call $\overline{f(t)\,c(t)}$ the turbulent-zone *contribution* to the conventional average $\overline{f(t)}$: $\overline{f(t)\,c(t)}/\overline{c(t)}$ is the turbulent-zone *average*. Obviously the sum of the turbulent-zone contribution $\overline{f(t)\,c(t)}$ and the non-turbulent (irrotational) zone contribution $\overline{f(t)}\,[1-\overline{c(t)}]$ is $\overline{f(t)}$ itself. In our work fluctuations are defined with respect to the conventional-mean velocity, so that the above addition law applies: defining fluctuations with respect to zone-average velocities ignores the fundamental velocity excursion in the zone.

Methods of making turbulent/non-turbulent decisions by examining $f(t)$, or otherwise, are discussed by Bradshaw & Murlis (1974) and Muck (1980); in the present work $f(t)$ is the signal either from a hot-wire anemometer or from a 'cold-wire' resistance thermometer in a boundary layer whose turbulent regions are marked by heating the surface slightly. An alternative approach to conditional sampling, used by Falco (1974, 1977) following the earlier work of Fiedler & Head (1966) is to use flow visualization, filling the whole of the turbulent region of an air flow with smoke, so that the interface can be distinguished. Falco, and also Head & Bandyopadhyay (1981) have used flow visualization with simultaneous hot-wire measurements: the present conditionally sampled hot-wire measurements substantiate their picture of the behaviour of low-Reynolds-number boundary-layer flows, although our interpretation of the results differs somewhat. This general agreement between the results of two different techniques gives one confidence in both. It should, however, be noted that smoke-flow visualization and conditional sampling of probe signals have one difficulty in common: inability to identify the position of the viscous superlayer precisely. In the case of conditional sampling the difficulty is just an *operational* one, our uncertainty about the choice of algorithm to be used in discriminating between turbulent and non-turbulent fluid (whether a velocity fluctuation signal or a temperature signal is used). The ratio of molecular diffusivity of momentum or vorticity to that of heat – the Prandtl number – is close enough to unity for the instantaneous boundaries of the 'hot' and 'turbulent' regions to be effectively coincident, and we shall see that it is much easier to base turbulent/non-turbulent decisions on a temperature signal than on a velocity signal. In the case of smoke-flow visualization, however, the ratio of viscosity of the fluid to the diffusivity of the contaminant, smoke – the Schmidt number – is extremely high, so that, in effect, the smoke does not migrate out further than the inner edge of the viscous superlayer. This *physical* difficulty means that some of the deep but narrow fissures seen in smoke pictures of turbulent flows may, although free of smoke, in fact contain significant vorticity (or heat) and should therefore count as turbulence according to probe measurements. Thus, while any consistent errors in conditional sampling measurements based on temperature-probe signals (or velocity-probe signals) ought not to

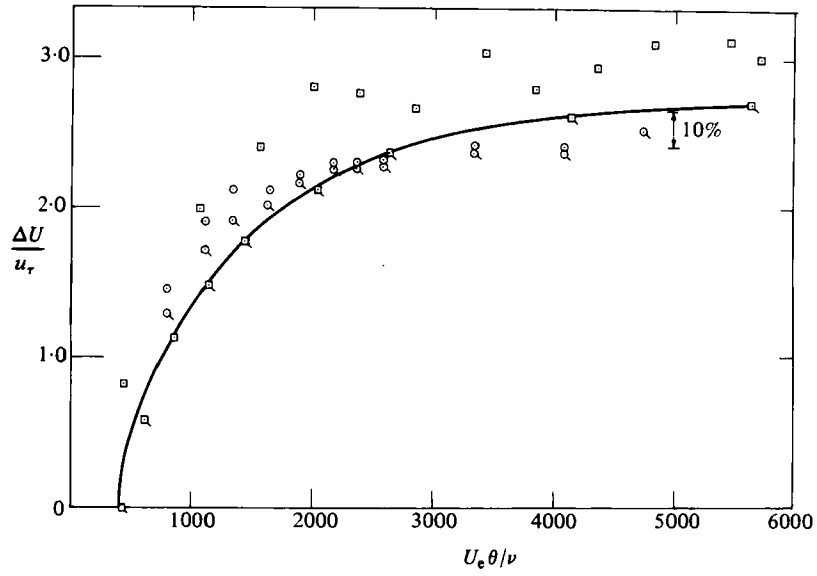

FIGURE 2. Variation of 'wake' strength with Reynolds number: ——, Coles (1962) best fit to data; ⊡, Coles (1962) analysis of Wieghardt data, $c = 5{\cdot}0$; ⊡, Coles & Hirst (1969) analysis of Wieghardt data; ⊙, present data, $c = 5{\cdot}2$; ⊙, present data, best-fit c.

depend significantly on Reynolds number, so that the Reynolds-number dependence of the measurements described below can be taken as real, at least in a qualitative sense, there is some *a priori* doubt about the validity of interpretation of smoke pictures. However, our one-point conditional sampling results and the multi-point conditional sampling measurements of Brown & Thomas (1977) both imply the presence of large, deep fissures between successive large-scale motions like those seen in the smoke pictures, representing real intrusions of irrotational fluid into the turbulent region.

Coles (1962) produced a simple plot showing the effect of Reynolds number on the velocity-defect profile in terms of the 'wake parameter' Π, defined by the velocity-profile formula

$$\frac{u}{u_\tau} = \frac{1}{\kappa}\ln\frac{u_\tau y}{\nu} + c\frac{\Pi}{\kappa}w\left(\frac{y}{\delta}\right), \tag{2}$$

with the additional restriction that $w(1)$ is equal to 2. Several forms of the wake function have been presented by different authors; the most flexible seems to be the cubic originally due to Finley, Phoe & Poh (1966) and discussed in detail by Dean (1977). In the analysis of experimental data $2\Pi/\kappa$ is most conveniently defined as the maximum deviation of the axial velocity profile from an extrapolation of the logarithmic law of the wall (figure 1). Figure 2 shows the variation of Π with Re_θ from the experiments of Wieghardt (1944), quoted by Coles as being nearest the consensus of reliable data. It may be noted that the disappearance of the wake parameter at low Reynolds number implies that the skin friction is about 15% higher than if (1) continued to hold, so low-Reynolds-number effects are of considerable practical importance, particularly in wind-tunnel model testing. Also, it should be noted that the point at which Π reaches zero is not necessarily the lowest Reynolds number at which turbulent flow can be maintained; Π is just a geometrical parameter, and in some boundary layers, including flows with free-stream turbulence, Π can be negative even though the flow is undoubtedly fully turbulent.

Simpson (1970) suggested that the changes in profile shapes, which Coles correlated in terms of Π, could equally well be explained by changes in the law of the wall, but Green (1971), Huffman & Bradshaw (1972) and Purtell, Klebanoff & Buckley (1981) have concluded that Simpson's suggestion is implausible. The law of the wall operates satisfactorily over a rather wide range of outer-layer conditions imposed by arbitrary pressure gradients, and it would seem extremely unlikely that mere changes in bulk Reynolds number would affect the scaling. A further implied challenge to Coles' analysis was put forward by Bushnell, Cary & Holley (1975), who analysed existing data to deduce that, in some supersonic wind tunnels, wall boundary-layer measurements showed a decrease in mixing length (or eddy viscosity) in the outer layer as Reynolds number decreases, in contrast to the increase in mixing length found on flat plates and corresponding to the decrease in Π. Recent work by Inman & Bradshaw (1981) has failed to reproduce the decrease in mixing length on wind tunnel walls at low speeds, and it appears to be an effect of the expansion in supersonic tunnel nozzles on the turbulence structure (Bradshaw 1974).

There are few detailed turbulence measurements available in low-Reynolds-number boundary layers, although Purtell *et al.* have presented measurements of u-component fluctuations and spectra. Falco and Head & Bandyopadhyay have made limited hot-wire measurements in conjunction with smoke observations. The restriction of the smoke work to low Reynolds numbers was an inevitable feature of the use of a low-speed smoke tunnel, rather than an intentional aim of the investigations, which did not examine the relation of the results to the Reynolds-number effects documented by Coles. The object of the present work, which started at about the same time as Falco's, was to produce an extensive set of basic turbulence measurements for low-Reynolds-number flows, and to apply modern conditional-sampling techniques to the study of the viscous superlayer so as to investigate the Huffman/Bradshaw hypothesis that it is indeed the superlayer that is mainly responsible for the low-Reynolds-number effects on the velocity profile documented by Coles. For simplicity, the work has been restricted to flows in zero pressure gradient. It is not likely that there will be a strong nonlinear interaction between the effects of low Reynolds number and those of pressure gradient, so that a well-founded method of correlating low-Reynolds-number effects in a constant-pressure boundary layer should be directly usable in a calculation method for boundary layers in arbitrary pressure gradient.

2. Experimental arrangement

The measurements were made in the 30 in. × 5 in. (762 mm × 127 mm) blower wind tunnel of the Department of Aeronautics at Imperial College (Bradshaw 1972). The work was done in two stages: the velocity-field measurements were made by Murlis (1975) and the temperature-intermittency measurements were made by Tsai in 1978/79. The arrangements for the two experiments were effectively identical. The working section of the tunnel, which has a total length of 9·5 ft (2·4 m), has a flexible roof for control of the pressure gradient, and in the present experiments the pressure gradient was set equal to zero. The nominal tunnel speed was 50 ft/s (15·3 m/s). The free-stream turbulence level was less than 0·1 %. The wind-tunnel contraction boundary layer was removed through a slot at the start of the working section and the test boundary layer began at a sharp leading edge. A 0·03 in. (0·076 cm) trip wire was fitted 0·5 in. (1·3 cm) downstream of the leading edge. In the 1978/79 experiments, the trip wire was insulated from the aluminium floor plate with mica, flush with the

surface, and used for heating the boundary layer. The electrical power input was 320 W. The floor plate was fitted with 3·5 in. (8·89 cm) diameter instrument ports at intervals of 6 in. (15·24 cm) on the centreline; traverse gear, surface tubes, etc. were mounted on plugs fitting flush with the surface. Preston surface Pitot tubes with diameters from 0·058 in. (0·147 cm) to 0·113 in. (0·287 cm) were used, together with fence-type Stanton tubes with a height h of about 0·002 in. (0·05 mm) and $u_\tau h/\nu \approx 2$. The Preston tubes were calibrated using Patel's (1965) law. Stanton tubes were calibrated against the Preston tubes in a high-Reynolds-number flow. Agreement between the skin-friction values indicated by different Preston tubes was 1 % or better at the higher Reynolds numbers. Mean-velocity profiles were measured using a round-section Pitot tube with an external diameter of 0·04 in. (1 mm) connected to a Combist micromanometer and a paper-tape data logger.

Measurements of u- and v-component velocity fluctuations were made using DISA Type 55A38 X-array hot-wire probes, operated at constant temperature at a resistance ratio of 1·8. The wire length $l = 1$ mm gives $u_\tau l/\nu \approx 30$ – that is, the wire length is roughly equal to the viscous sublayer thickness, and considerably smaller than Falco's 'typical eddies', *at any Reynolds number*. Probes were individually calibrated, assuming a King's law velocity exponent of 0·45; yaw calibration results were fitted to an effective cosine law, as described by Bradshaw (1971).

Temperature-fluctuation measurements were made with 1 μm diameter platinum wires, about 1 mm long, operated at a constant current of about 1 μA, the signal being amplified by a Brookdeal type 931 low-noise preamplifier before compensation for thermal inertia by a standard resistance–capacitance operational amplifier network. Compensation was set, approximately, in real time so that the compensated temperature signal at the end of a 'hot' zone returned as quickly as possible to the background temperature without actually overshooting; this technique has been used satisfactorily in other experiments, and does not seem to hamper detection of the viscous superlayer. The output from the hot-wire or cold-wire electronics was high-pass filtered at 1 Hz and low-pass filtered at 20 kHz, and the fluctuating component was recorded by an Ampex FR 1300 FM tape recorder with a bandwidth of 20 kHz at 60 in./sec. The analog tape recordings were later replayed at a lower speed, digitized, at an equivalent real-time rate of 40000 samples/s per channel, and analysed on the Imperial College Computer Centre's CDC machines, using a version of the program described by Weir & Bradshaw (1974). Pitot and hot-wire probe tips were approximately 1·4 in. (3·5 cm) ahead of the surface-tube positions so that the Reynolds numbers for skin friction measurements ($750 < Re_\theta < 6000$) are slightly higher than those for the nearest corresponding probe profiles.

Digital analysis of the velocity and temperature fluctuations used routines (the 'intermittency schemes') designed to identify turbulent/irrotational interfaces. The conditional-average velocity-fluctuation measurements presented here were made in an isothermal flow, the intermittency being obtained from the velocity fluctuations. The temperature-intermittency and zone-length statistics presented here were obtained in the later measurements in heated flow, and no velocity-fluctuation measurements were made in that case. We regard the 'temperature-intermittency' scheme as the only acceptable one for measuring zone-length statistics: however we believe that 'velocity-intermittency' schemes are adequate for evaluating zonal contributions to turbulence statistics. Since the present paper is the first attempt at reconciliation of flow visualization and intermittency statistics, and since published zone-length statistics vary greatly according to the intermittency algorithm used, a detailed discussion is necessary.

Our discrimination scheme for the velocity field (the 'velocity scheme') uses the instantaneous product uv, whose time mean $\overline{uv}$ gives the local turbulent shear stress. The pragmatic justification for using uv rather than either u or v separately is that the main object of the investigation was to examine the shear-stress-producing mechanism in the turbulence. Therefore, providing that regions with large contributions to $\overline{uv}$ could be satisfactorily identified, the effect of inaccuracy of the intermittency scheme on the final conditional-average results should be comparatively small; this point was in fact checked by Murlis. Also, uv is comparatively small (although not identically zero) in the irrotational fluid, and is therefore a reasonable choice for a discrimination signal. The intermittency scheme is basically that devised by Castro (1973; see also Castro & Bradshaw 1976); turbulence is registered if either the first or the second time derivative of the instantaneous uv exceeds a chosen threshold, different in each case. Frequency response and spatial resolution of the hot wires are inadequate to give the second, or even the first, time derivative with high accuracy: it is therefore essential to base the threshold levels on the actual r.m.s. (or rectified-mean) values of duv/dt and d^2uv/dt^2 in the turbulent regions. This makes the measured intermittency slightly more sensitive to the threshold value than if the threshold were chosen absolutely, but reduces dependence of the results on the analogue frequency response or the digital sampling interval (Muck 1980). It seems impracticable to choose a threshold for a velocity scheme simply as a multiple of the *non-turbulent* zone fluctuations.

The choice of discrimination function and thresholds for velocity-intermittency schemes is discussed in detail by Bradshaw & Murlis (1974) and Muck (1980): as will be seen below, the problems are very much less severe in temperature-intermittency schemes, because the temperature in a heated flow has the ideal property of being larger than the free-stream value everywhere within the turbulence. In contrast, almost any simple function of velocity that is supposed to be non-negative within the turbulence, even the square of the vorticity, will in fact have occasional zeros, either because it is derived from squaring or rectifying a function that changes sign or (espcially in the case of vorticity) because the function depends too strongly on the high-wavenumber velocity fluctuations, which are known to be intermittent even if the turbulence as a whole is not (Batchelor 1953; Sandborn 1959). These difficulties lead to the prediction of short irrotational regions within a turbulent zone. The usual practice of rejecting all such short regions suppresses the genuine consequences of the highly re-entrant nature of the interface, which is so clear in smoke pictures. Rejecting short regions by filtering the criterion function is unsatisfactory; as shown by Bradshaw & Murlis, it would produce inexact results even if the criterion function were the actual on/off intermittency function itself. In the present work we have chosen to employ two definitions for velocity-field intermittency:

(i) '*retail*' *intermittency*, derived from the unsmoothed criterion function without the application of any 'hold time' other than the digital sampling time interval (which is small); and

(ii) '*wholesale*' *intermittency*, in which short turbulent regions far from any long turbulent region are ignored altogether as being due to noise, eccentricities of the algorithm, or unimportant glancing encounters with turbulent regions; while short turbulent regions adjacent to a long turbulent region are regarded as merging with it and short irrotational regions within a turbulent zone are ignored, so that the scheme is 'turbulence-biased'.

Figure 3 gives details of the velocity-intermittency routine: the treatment of short excursions by the 'wholesale' scheme can be understood by comparing the two

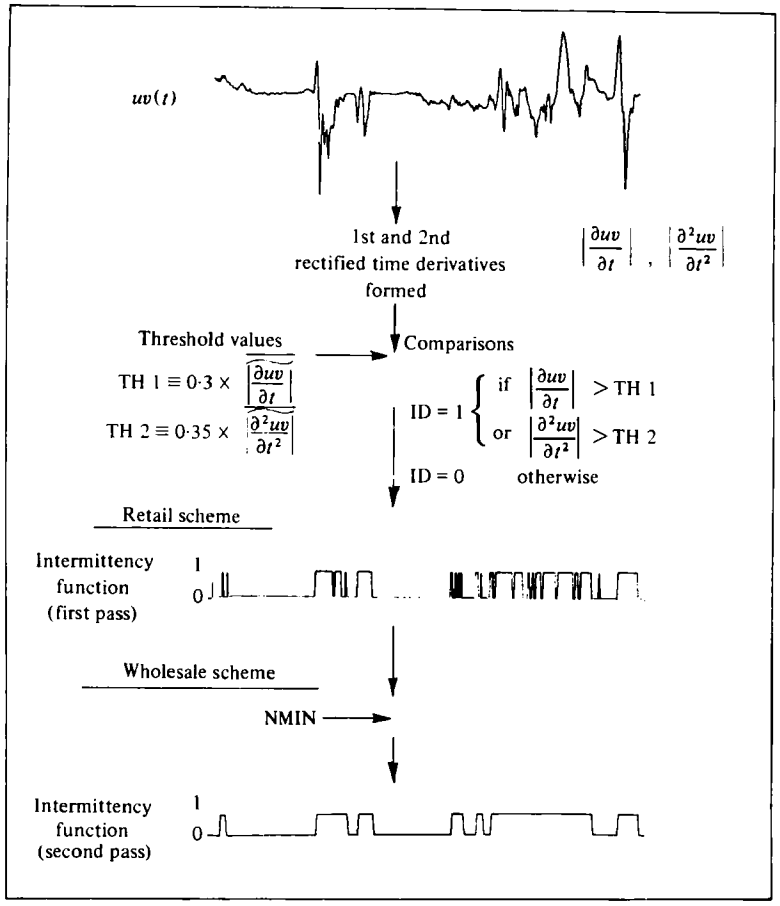

FIGURE 3. Velocity-intermittency scheme. First pass, 'retail'; intermittency function ID set equal to 0 or 1. Second pass, 'wholesale'; intervals less than NMIN times sampling interval set equal to 1 if irrotational, 0 if turbulent.

intermittency-function plots, especially near their right-hand ends. The thresholds for the first and second time derivatives of uv were set at respectively 0·24 and 0·28 of the turbulent-zone rectified mean of these quantities, and NMIN, the length of the smallest region to be given special treatment, was taken as 5 sampling intervals, corresponding to a streamwise distance $L_{\min}$ of 0·075 in., or about $0{\cdot}05\delta$ at the highest Reynolds number. Note that $u_\tau L_{\min}/\nu \approx 60$; $L_{\min}$ is small compared with the size of a 'typical eddy'. Note also that if the medium-to-small-scale structure does scale on the slowly varying quantity ν/u_τ as previous workers have found, a constant $L_{\min}$ is less likely to cause spurious variation of the results with Reynolds number (i.e. x) than a constant $L_{\min}/\delta$. The thresholds in the velocity-intermittency scheme were chosen so as to give good agreement with the measurements of Klebanoff (1955) in the outer part of the boundary layer, but the intermittency close to the surface asymptotes to a value significantly less than unity, about 0·94 for the 'wholesale' scheme and about 0·86 for the 'retail' scheme with its larger number of dubious irrotational 'dropouts'. This faithfully reflects the fact that the spatial distribution of uv is itself rather patchy, apparently to a greater extent than would be expected from the product of uncorrelated Gaussian variables. It can be argued that the values of intermittency found by using the uv-criterion are in fact the best for our purpose – conditional sampling of the shear-stress production processes. Even if the

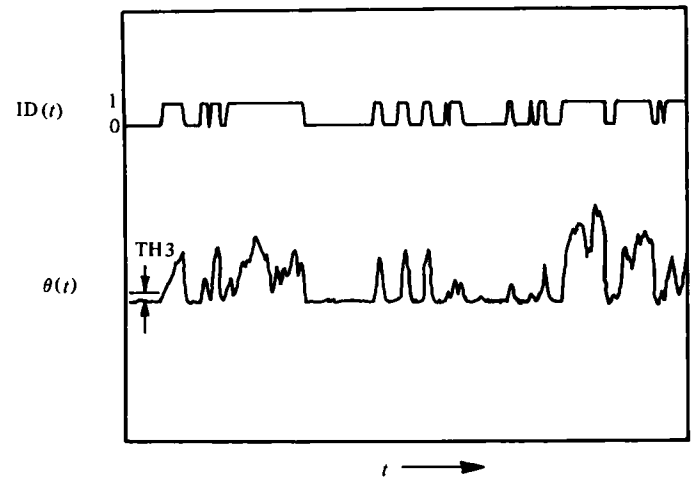

FIGURE 4. Temperature-intermittency scheme. ID set equal to 1 if temperature exceeds local 'cold' level by more than TH3. Precautionary scheme to allow for changes in 'cold' level operated only rarely in this experiment.

argument is not accepted, it is certainly true that the turbulent-zone contributions to second- and third-order velocity products are very insensitive to the presence or absence of the short 'dropouts'. Trouble with dropouts is *not* confined to uv: when v^2 was used as an intermittency-criterion function the intermittency was always underestimated near the surface and overestimated near the edge of the boundary layer. In our trials, the scheme used by Hedley & Keffer (1974*a*), in which the criterion function is the sum of the square of the time derivatives of u and v, was more satisfactory than v^2 but less satisfactory than uv (Muck 1980). We conclude that the more obvious schemes for deducing the intermittency from single-point velocity measurements are unlikely to give sufficiently good results for detailed examination of intermittency statistics.

A more generally satisfactory method of measuring intermittency is to contaminate the turbulent flow with heat, smoke, or dye. LaRue & Libby (1974), Dean & Bradshaw (1976) and Chen & Blackwelder (1978) have successfully used temperature. In principle all that is necessary is a simple level criterion, with the threshold set just above the typical noise level in the background flow (caused by electronic noise or by free-stream temperature fluctuations). The present scheme, described in more detail by Weir, Wood & Bradshaw (1981), is based on a level criterion but contains various refinements like allowances for unsteadiness of free-stream temperature. Chen & Blackwelder found a strong and monotonic variation of temperature intermittency with threshold level, but it can be seen from the temperature traces reproduced in their paper that their signal was noisy and either lacking in frequency response or significantly undercompensated. Figure 4 shows a typical temperature trace from the present experiment: $\partial\theta/\partial t$ is seen to be numerically large at the start and end of each excursion so that the intermittency and zone length depends only weakly on the threshold level TH3 (see table 1). The temperature-intermittency algorithm contains an option by which irrotational (cold) regions occupying less than NMIN sampling intervals can be ignored. Zone-length statistics for different choices of NMIN will be given below, but it should be noted that the temperature-intermittency scheme is essentially immune to the spurious 'dropouts' that plague velocity-intermittency schemes.

There is at present some controversy about the best method of presenting results

	Threshold value TH3 (°C)	γ_θ	$\frac{\hat{f}\delta_{995}}{U_\infty}$	$\frac{\hat{L}}{\delta_{995}}$
$y/\delta = 0{\cdot}69$	0·22	0·9184	0·646	1·346
	0·20	0·9204	0·644	1·353
	0·18	0·9211	0·643	1·355
	0·15	0·9196	0·680	1·280
	0·12	0·9190	0·721	1·206
$y/\delta = 1{\cdot}00$	0·22	0·2549	0·861	0·2951
	0·20	0·2555	0·860	0·2959
	0·18	0·2560	0·856	0·2979
	0·15	0·2582	0·859	0·2995
	0·12	0·2614	0·861	0·3027

TABLE 1. Temperature-intermittency results – sensitivity to threshold value (see figure 4). The above values are all from the same data and the same data points in each case. $Re_\theta = 1880$. A typical 'noise' level θ_1 is about 0·1 °C or less.

for zone-length distributions. Several previous papers quote an 'average burst frequency', but it is easy to see that the presence of a small irrotational interval in the middle of each turbulent burst would double the burst frequency; such irrotational intervals would be embarrassing if spurious, and almost irrelevant if real. To quote a single 'burst frequency' for measurements in the intermittent region is no more sensible than quoting a single frequency for the velocity fluctuations within the flow, which in fact have a broad-band spectrum. Following Corrsin & Kistler (1955), we have chosen to present probability distribution functions of zone length: Chevray & Tutu (1978) have presented zone-length probability distributions in a turbulent jet. If necessary, weighted-average zone lengths can be defined in terms of integral moments of the probability distribution. Also, probability distributions conditional on the smallest accepted zone length $L_{\min}$ can be produced, and we shall see below that the effect of $L_{\min}$ is extremely large.

Since the object of the present investigation is to study the behaviour of the shear stress, the measurements were confined to the u- and v-components and no attempt has been made to measure the w (spanwise) component of velocity. For the purpose of estimating advection in the turbulent energy equation, we have assumed that $\overline{w^2}$ is the average of $\overline{u^2}$ and $\overline{v^2}$. This method does beg the question of variations of $\overline{w^2}/\overline{u^2}$ with Reynolds number, but the error involved in the calculation of advection should be fairly small.

3. Results and discussion

3.1. *Skin-friction coefficient*

Figure 5 shows the skin-friction coefficient obtained by the Preston tubes and the Stanton fence device, and it may be seen that a very close correspondence exists between the data sets throughout the experimental Reynolds-number range. The Preston tube calibration assumes the validity of the logarithmic law-of-the-wall velocity profile, while the Stanton device, being sufficiently small to remain nominally within the viscous sublayer, should be almost independent of any changes in the logarithmic law. Thus agreement between the two devices is strong evidence for the validity of the logarithmic law of the wall down to a Reynolds number as low as

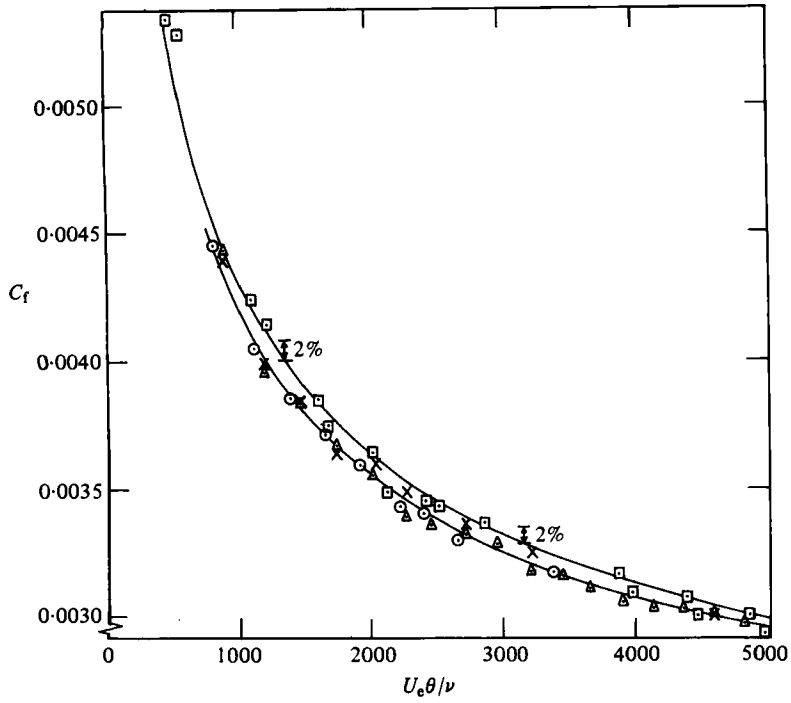

FIGURE 5. Variation of skin-friction coefficient with Reynolds number: ⊙, traverse Pitot tube on surface; △, Preston tube; ×, Stanton tube; ⊡, Coles analysis of Wieghardt data, $c = 5{\cdot}0$.

$Re_\theta = 700$. It does not necessarily refute Simpson's suggestion that the Kármán constant changes with Reynolds number, because he postulated a compensating change in the intercept in the logarithmic law which would leave the velocity in the range occupied by the logarithmic law almost unaltered. Figure 5 also shows the skin-friction results obtained by Coles & Hirst (1969) from the data of Wieghardt (1944). There is a consistent difference between the two data sets, the present results lying about 2% below Wieghardt's. The reason for this is that, as pointed out by Brederode & Bradshaw (1978), Coles & Hirst used logarithmic-law constants $\kappa = 0{\cdot}41$ and $c = 5{\cdot}0$, whereas the Patel (1965) Preston-tube calibration used here corresponds better to the assumption that c is equal to 5·2. Coles's choice of 5·0 was an indirect one whereas Patel's Preston-tube calibration is based on careful measurements in pipe flows, and the implied value of c therefore carries considerable weight. If Wieghardt's results were reprocessed using $c = 5{\cdot}2$, they would agree almost exactly with the present ones and can therefore be taken as definitive.

3.2. *Mean-velocity profiles*

Figure 6 shows mean-velocity profiles for each measurement station corresponding to a Reynolds-number range $800 < Re_\theta < 4750$, plotted in the familiar semilogarithmic form used in figure 1. The solid lines represent the logarithmic law with $\kappa = 0{\cdot}41$, $c = 5{\cdot}2$. The small discrepancies between the measurements and the logarithmic law at low Reynolds numbers are attributable to experimental error, since the use of Preston-tube values of skin friction would automatically force accurate velocity profiles to follow – or at least intersect – the logarithmic law. In order to evaluate the wake parameter for each profile (figure 2), the value of c was adjusted to give the best fit of the logarithmic law to the measured profile. This slightly reduces scatter

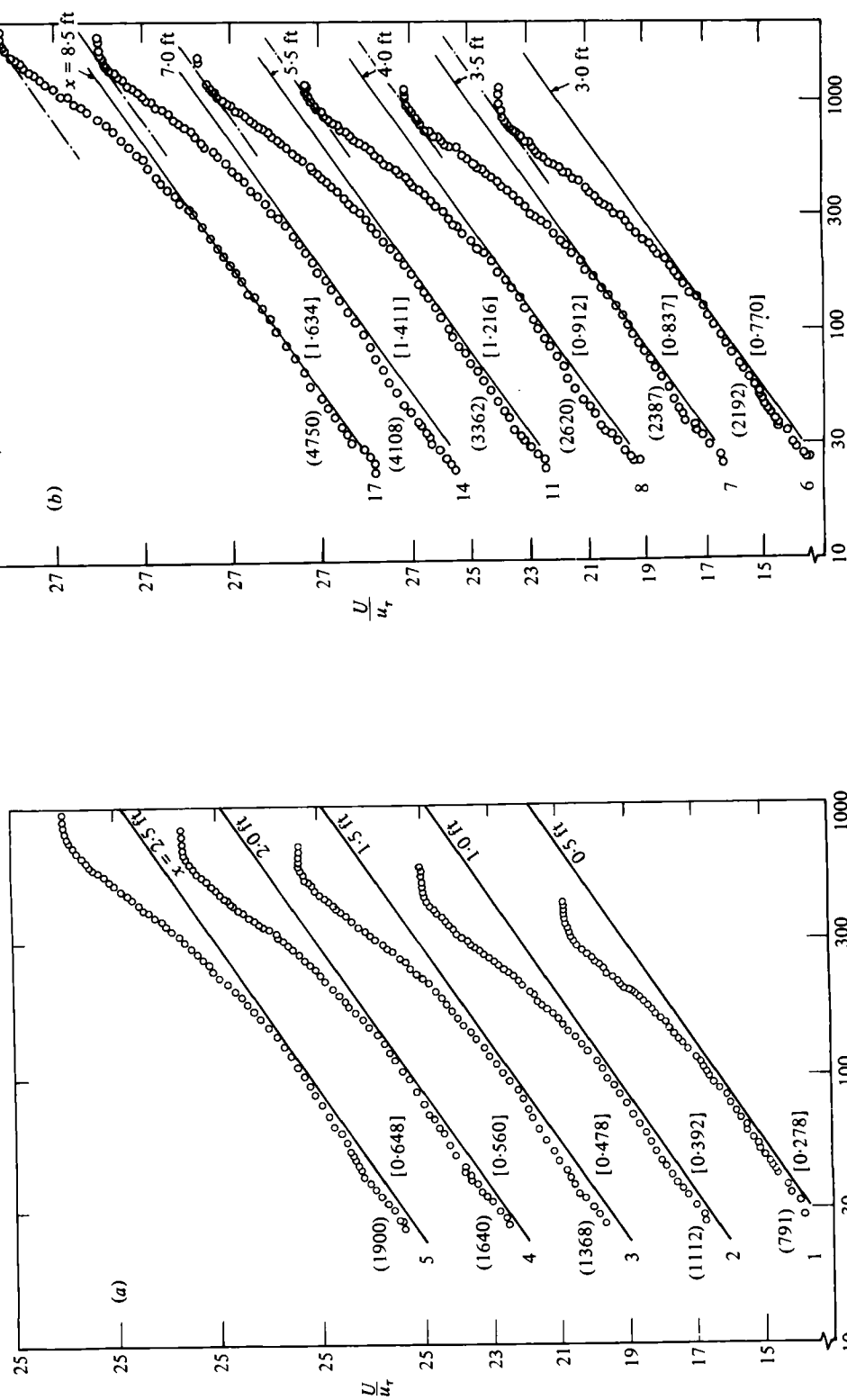

FIGURE 6. Mean-velocity profiles in semilogarithmic coordinates. Ordinate scale refers to lowest curve; other curves successively displaced upwards by 3·0 units. Labels in parentheses are values of $U_e\theta/\nu$, those in brackets are $\delta \equiv \delta_{99\cdot5}$ (ins.). (*a*) $x = 0{\cdot}5$–$2{\cdot}5$ ft (0·15–0·75 m); (*b*) $x = 3{\cdot}0$–$8{\cdot}5$ ft (0·9–2·55 m).

without altering trend: compare the tagged and plain circles in figure 2. The highest value of wake parameter obtained in the present results was still somewhat below the asymptotic value obtained by Wieghardt at high Reynolds number: Wieghardt's results suggest that the asymptotic value should be reached by $Re_\theta = 5000$, so there seems to be a real, but slight, difference between the two sets of results.

3.3. *Intermittency statistics*

Figure 7 shows various measurements of the intermittency factor at high Reynolds number. It can be seen that the temperature intermittency (for which our results agree very closely with those of other workers at Imperial College: see e.g. Andreopoulos 1978; Andreopoulos & Bradshaw 1980; Hancock 1980) is slightly larger than the intermittency measured by Klebanoff (1955); in our results $\gamma = 0{\cdot}5$ is reached at $y \equiv Y = 0{\cdot}9\delta_{995}$ approximately, whereas Klebanoff's results imply $Y/\delta = 0{\cdot}86$, although his boundary-layer thickness is poorly defined. The way in which the velocity-intermittency factors, both wholesale and retail, asymptote to values below unity is clearly seen, and although the outer-layer values of velocity intermittency are quite acceptable they will not be used further in the present discussion. Temperature-intermittency measurements at the lower Reynolds numbers are almost indistinguishable from those shown in figure 7. Differences are nowhere more than about $\pm 0{\cdot}02$ in γ, and the only possibility of a real trend with Reynolds number is a hint that the intermittency factor starts to decrease from unity at a smaller value of y/δ at the higher Reynolds numbers. Evidently the intermittency factor as such will not yield any clue as to the origin of the low-Reynolds-number effects. In view of the large differences in interface statistics so obvious from smoke pictures, and indeed from the zone-length probability distributions below, the imperturbability of the intermittency distribution is surprising and at once suggests that the large eddies are relatively independent of Reynolds number.

Conditionally sampled mean velocities using the 'retail' velocity intermittency are shown in figures 8 and 9, and compared with the results obtained by Hedley & Keffer (1974*b*). The notation introduced by Kovasznay, Kibens & Blackwelder (1970) is used: $\overline{\sim}$ denotes a turbulent-zone average (not a 'contribution' in this case), and $\overline{\simeq}$ an irrotational-zone average. Hedley & Keffer's results generally agree well with those of Kovasznay *et al.*; except that their turbulent-zone U-component mean velocity is rather lower than that of Kovasznay *et al.* The present results agree fairly well with those of Hedley & Keffer in the outer region, $y/\delta > 0{\cdot}6$ say – our turbulent-zone U-component velocity agrees better with that of Kovasznay *et al.* – but nearer the surface the present conditional-average velocities have all approached the conventional-average velocity, whereas the irrotational-zone average measured by Hedley & Keffer and by Kovasznay *et al.* remains significantly different from the overall mean velocity. The *turbulent*-zone U-component velocity must, of course, equal the overall mean velocity when the intermittency factor is unity; the discrepancy in our irrotational-zone average is attributable to the underestimate of intermittency provided by the velocity-intermittency scheme, so that our irrotational-zone results are too close to the turbulent-zone velocity. However, the fact that the present results for this critical test agree tolerably well with those of past investigators in the outer part of the boundary layer indicates that the present velocity-intermittency scheme should also give acceptable conditional averages for turbulence quantities in the outer layer.

It is more difficult to validate the present measurements of zone-length statistics by comparison with the results of other workers at high Reynolds number, because

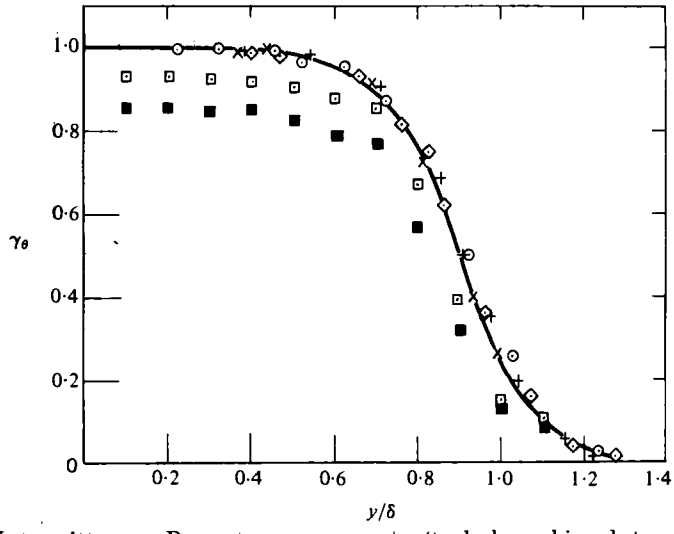

FIGURE 7. Intermittency. Present measurements (turbulence-biased temperature scheme) at indicated values of $U_e\theta/\nu$: +, 1100; ×, 1880, ⊙, 2430; ◇, 4820. ——, error function $\overline{Y} = 0{\cdot}9\delta$. Velocity scheme: ■, 'retail'; ⊡, 'wholesale'; both at $U_e\theta/\nu = 4750$.

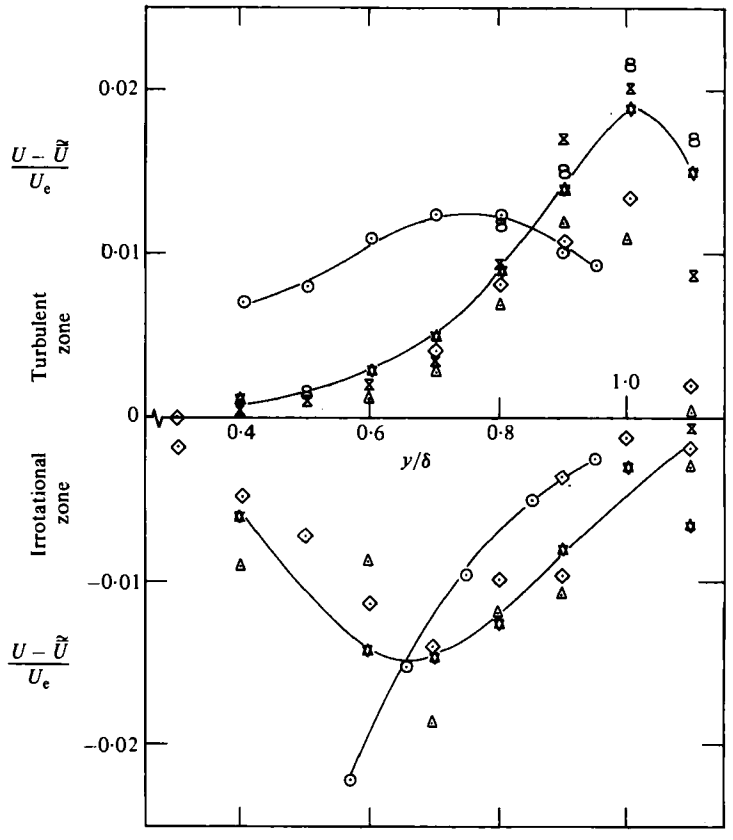

FIGURE 8. Zone-averaged U-component velocity ('retail' velocity scheme for intermittency) at indicated values of $U_e\theta/\nu$: △, 791; ◇, 1112; ⧖, 1368; 8, 1900; ✡, 4750; ——○——, Hedley & Keffer (1974*b*), 9700. Values are plotted with respect to conventional mean U.

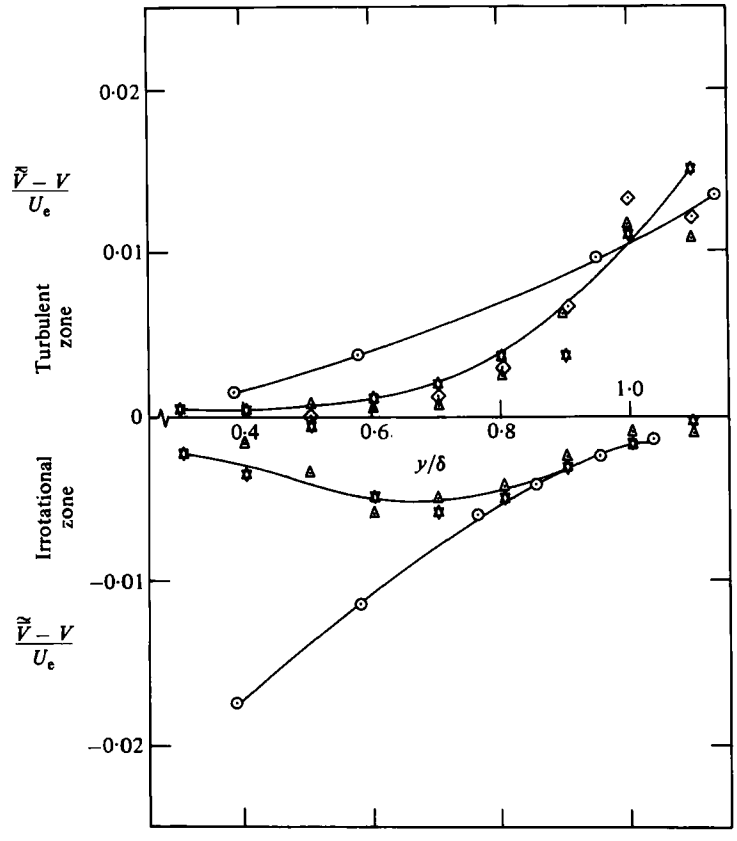

FIGURE 9. Zone-averaged V-component velocity. Symbols as in figure 8. Values are plotted with respect to conventional mean V.

of the extraordinary diversity of those results. 'Typical burst lengths', however defined, usually depend very strongly on the threshold levels used in velocity-intermittency determination schemes (e.g. Hedley & Keffer 1974*a*). As remarked above, Chen & Blackwelder (1978) show quite large effects of threshold level even on temperature-intermittency statistics, but this is believed to be due to inadequate resolution of the temperature signal. The present investigation appears to be the only one in which both velocity and temperature intermittency have been measured. In order to compare the two types of intermittency more closely, we have analysed rough-surface data ($U_e\theta/\nu = 22000, c_f = 0{\cdot}0052$) originally acquired by Andreopoulos (1978), and typical results are shown in figure 10, of which part (*b*) is a continuation of part (*a*). This shows the temperature trace, the u- and v-component velocity traces, the uv-product on which the velocity intermittency scheme is based, and the unit on/off intermittency function signals for the three types of intermittency. The vertical scale is arbitrary. It is clear that the temperature-intermittency function corresponds accurately to the temperature signal; the question of whether the minor 'dropouts' are real irrotational fissures or simply newly turbulent fluid whose temperature has not yet much increased is virtually impossible to settle. This is a comparatively minor point; a more important influence on the temperature intermittency is the presence of short isolated regions of excusion in temperature like that at about 560 time units. This is undoubtedly a small wisp of turbulence and corresponding excursions in u and v can be seen: unfortunately, it scarcely shows up

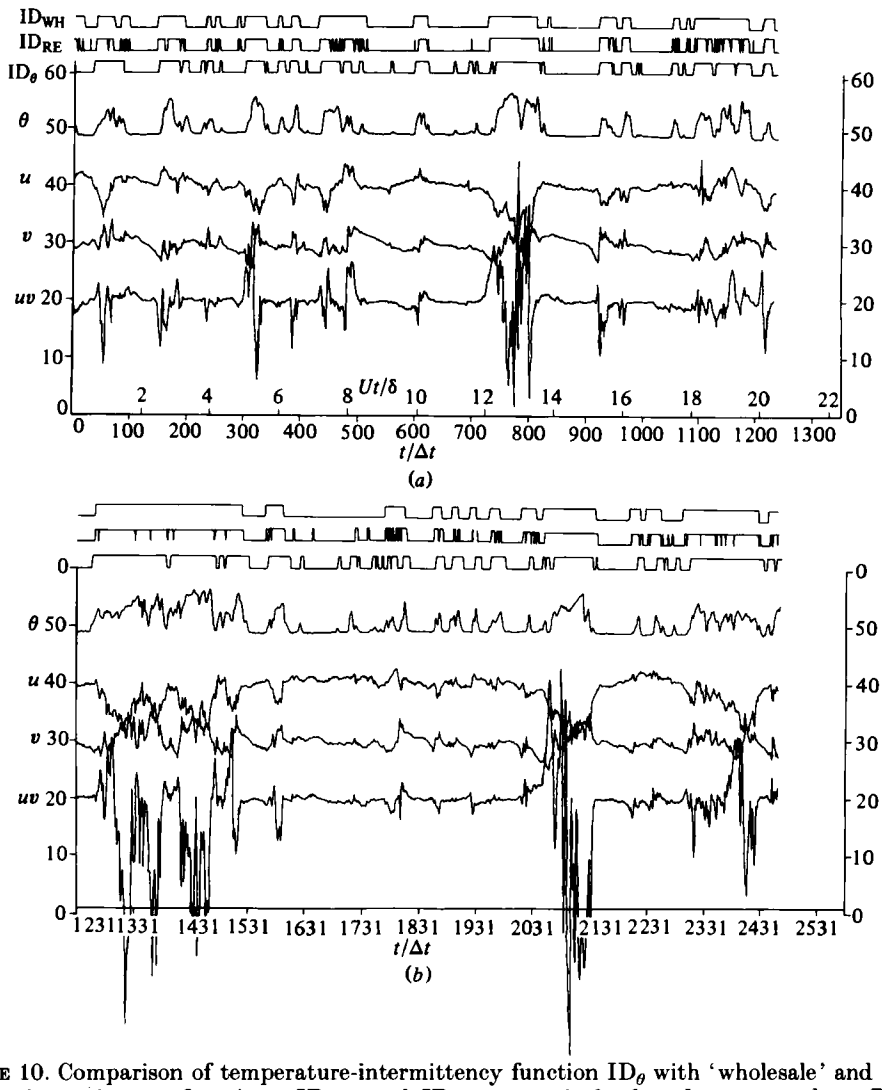

FIGURE 10. Comparison of temperature-intermittency function ID_θ with 'wholesale' and 'retail' velocity intermittency functions, ID_{WH} and ID_{RE} respectively, based on uv-product. Data of Andreopoulos (1978), $U_e\theta/\nu = 22000$ (rough surface), $y/\delta = 0{\cdot}89$, $\gamma \approx 0{\cdot}5$; L_{min}/δ for 'wholesale' intermittency $0{\cdot}1\delta$, sampling interval $0{\cdot}017\delta$ (i.e. $\Delta t = 0{\cdot}017\delta/U_e$).

on uv and is not detected by the velocity-intermittency scheme. In contrast, the gradient or second gradient of uv near 840 time units is large enough to produce two short spikes in the retail velocity intermittency, but does not correspond to any excursion of temperature, and is therefore evidently a region of unusually high irrotational velocity fluctuation. A final source of difference between velocity and temperature intermittency is the quite frequent presence of temperature excursions, at 670 time units for example, which do *not* correspond to turbulent velocity signals: these are evidentally wisps of turbulence like the one referred to above, in a late stage of decay, and whether they are counted as real depends upon one's interests and prejudices. The way in which the 'wholesale' scheme merges or suppresses the short 'spikes' seen on the retail record is clear. Unfortunately the retail spike at about 700 time units, which has been eliminated from the wholesale-intermittency function trace, corresponds to an unmistakable excursion in temperature and is therefore real

turbulence. For the most part the wholesale-intermittency-function trace corresponds quite well with the temperature intermittency, but the quantitative discrepancies are significant. We proceed to discuss the quantitative zone-length statistics obtained by the different schemes.

It is important to realize that all the interfacial statistics depend on the minimum turbulent and irrotational zone lengths recorded. For example, if a short irrotational 'dropouts' occurs in the middle of each turbulent zone the whole of the burst-length probability distribution is changed. The simplest method of presenting zone-length results is therefore as a conditional probability density function (p.d.f.) $P(L|L_{\min})$, where L is the zone length and $L_{\min}$ is the minimum length of turbulent or irrotational 'bursts' *counted*: in practice, one generates a series of zone-length probability distributions, one for each of the values of $L_{\min}$ considered. The results, of course, depend on the processing of events shorter than $L_{\min}$; the results below all use the 'turbulence-biased wholesale' scheme described in §2 and illustrated in figure 10. Typical results for the conditional p.d.f. of turbulent zone length are shown in figures 11*a*, *b*). Both plots were obtained from the same recording of u, v and θ data: note that, in order to convert *zone durations* to zone lengths, it has been assumed that the convection velocity is equal to the local mean velocity. The effect of minimum sample length ($L_{\min}$ in length, NMIN in terms of sampling interval) is more pronounced in the case of the velocity scheme than in the case of the temperature scheme but results at larger $L_{\min}$ agree fairly well. Almost everywhere, the effect of increasing $L_{\min}$ is to increase the probability at large L because of the elimination of 'dropouts' partitioning the turbulent zones. This can be seen immediately in figures 12(*a*, *b*), where the variation of the average zone lengths, burst frequencies, and intermittency factor are plotted against $L_{\min}$. Here $\hat{L}_t$ is the centroid of the p.d.f. for given $L_{\min}$, and $\hat{f}$ is $U/\hat{L}_t$: note that the frequency is made dimensionless with the free-stream velocity, and therefore differs from the reciprocal of L/δ by a factor of U/U_e. Moderate changes in $L_{\min}$ have very little effect on γ_θ but γ_u changes by about 0·07 over the range shown. Naturally, the average burst length changes significantly in both cases, but more in the case of the velocity scheme. Tolerable agreement between the two values of $\hat{L}_t$ is obtained only near $L_{\min} = 0{\cdot}1\delta$; γ_θ and γ_u agree best for $L_{\min} \approx 0{\cdot}05\delta$. Figure 13, which should be compared with figure 11 (*b*), shows the effect of retaining short turbulent bursts, while continuing to reject short irrotational dropouts: this of course increases the probability density at small values of L, but the changes at large L simply result from the necessary rescaling of the probability distribution so that its integral over L at any value of $L_{\min}$ is unity.

Although conditional p.d.f.s are a convenient means of presenting information about zone-length statistics, and of demonstrating the superiority of the temperature-intermittency scheme quantitatively, it has to be recognized that the basic problem is insoluble; we are trying to distinguish three-dimensional turbulent eruptions into the irrotational flow by means of measurements at only one y-position at a time and it is impossible to distinguish adjacent but isolated eddies from a series of closely spaced turbulent zones forming part of the same eddy. Similar, but less severe, problems appear even if two-dimensional information (e.g. smoke pictures) is available. However, conditional probability distributions of zone lengths can at least be reprocessed by other workers with different ideas of the 'correct' values of $L_{\min}$. It may be possible to present information more compactly than is done in figures 11 and 13; figure 14 shows that when L is normalized by $\hat{L}$ values of $\hat{L}P(L)$ for different values of $N_{\min}$ (represented by different symbols) collapse on the same curve, to an accuracy almost within that of the measurements. If this collapse is accepted, then

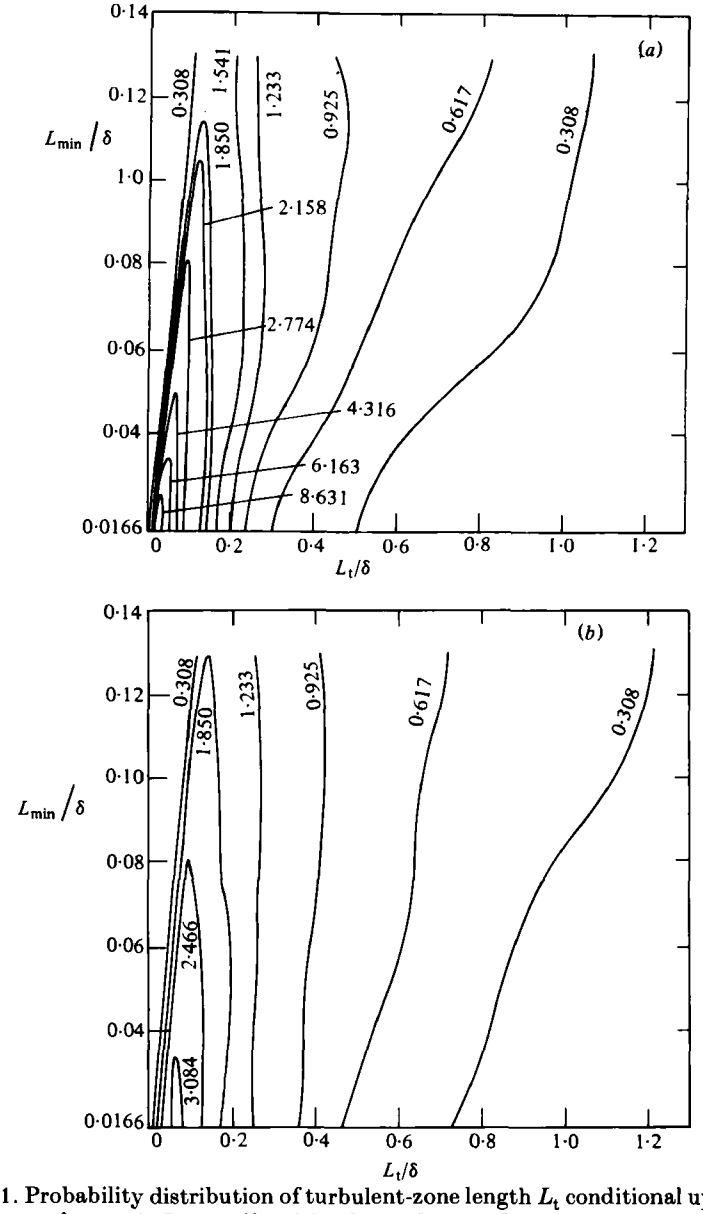

FIGURE 11. Probability distribution of turbulent-zone length L_t conditional upon length of shortest interval treated as real, L_{min}. $y/\delta = 0{\cdot}89$. Same data as figure 10. (*a*) Turbulence-biased velocity scheme; the distribution for $L_{min}/\delta = 0{\cdot}017$ (smallest interval length equal to one sampling interval) is the 'retail' one, and that for $L_{min}/\delta = 0{\cdot}1$ (NMIN = 5) is the 'wholesale' one. (*b*) Turbulence-biased temperature scheme.

the conditional probability distribution can be presented in the form of a curve like figure 14, together with a plot of $\bar{L}$ against L_{min} (figure 12). It would be unwise to read too much physical meaning into the collapse shown in figure 14; taken at face value it implies that the occurrence of dropouts is entirely random, but direct reasoning suggests that this is somewhat improbable, even in the case of spurious dropouts that are an artifact of the intermittency scheme. There is a small difference in the shapes of the curves at low *Re* (figure 14*a*) and high *Re* (figure 14*b*).

For the purposes of studying the effects of Reynolds number on the probability

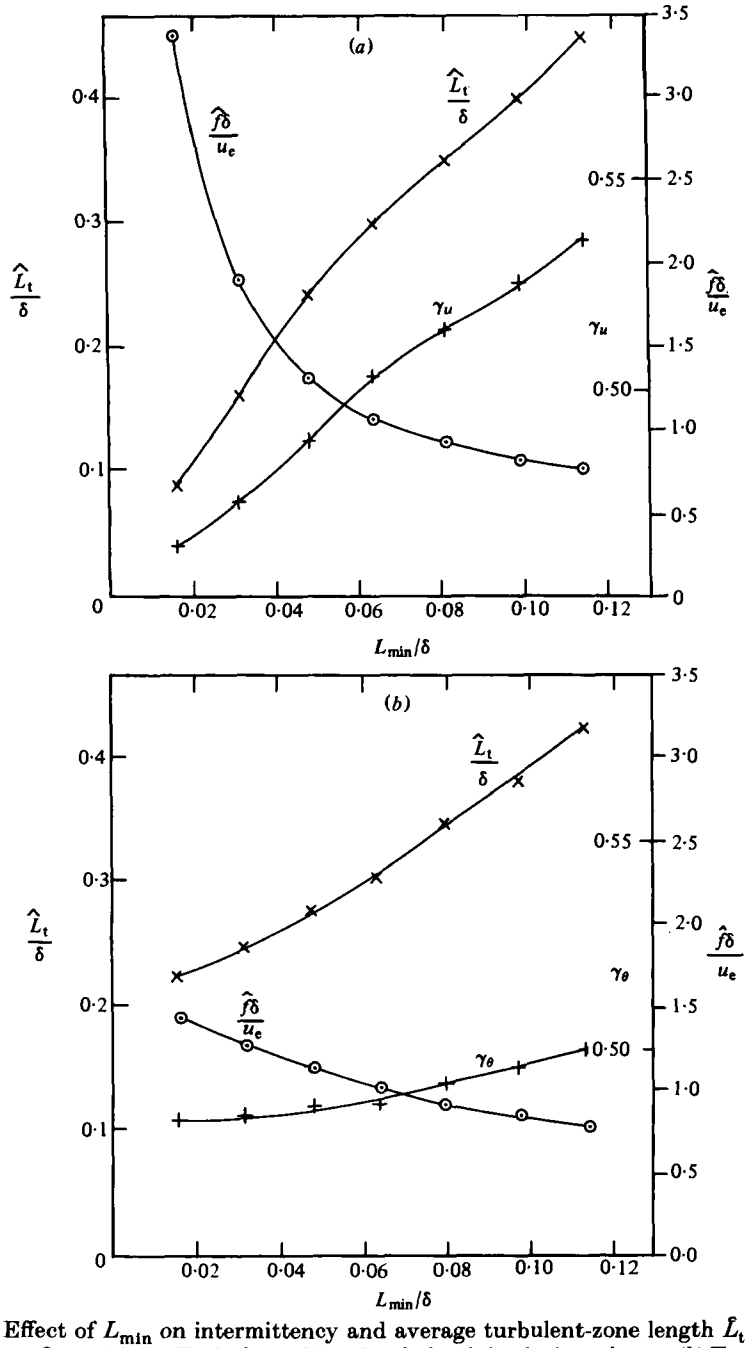

FIGURE 12. Effect of L_{min} on intermittency and average turbulent-zone length $\hat{L}_t$ and frequency $\hat{f}$. Same data as figure 10. (*a*) Turbulence-biased 'wholesale' velocity scheme. (*b*) Turbulence-biased temperature scheme.

distribution function, we have used the temperature intermittency routine with NMIN set equal to zero (strictly, to a length corresponding to one digital sampling interval). As was already noted by Corrsin & Kistler (1955), long sampling times are required to establish the probability of rare events – i.e. the occurrence of very long turbulent or irrotational zones. The measurements presented here were obtained using a sampling period of 4·6 s, corresponding to a streamwise travel time of at least

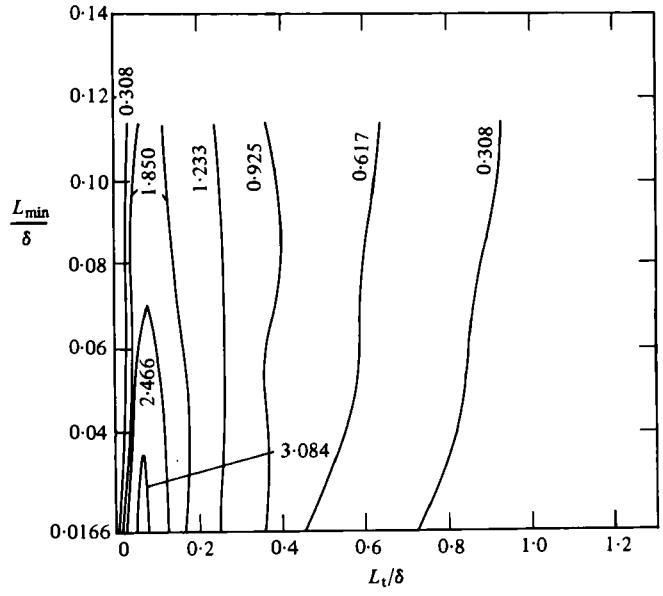

FIGURE 13. Conditional probability distribution of turbulent-zone length (temperature scheme), *including* all short turbulent zones; irrotational zones of length less than NMIN are ignored, as in figure 11(*b*). Same data as figure 10.

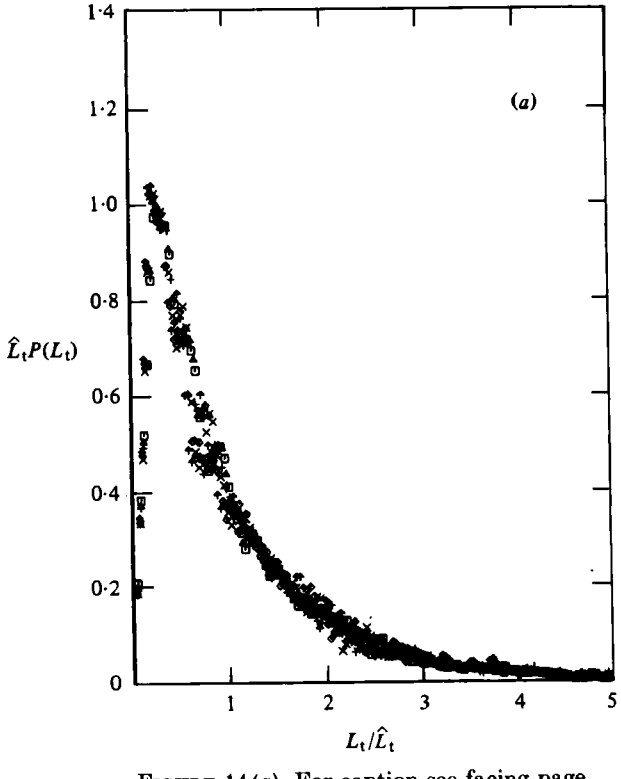

FIGURE 14(*a*). For caption see facing page.

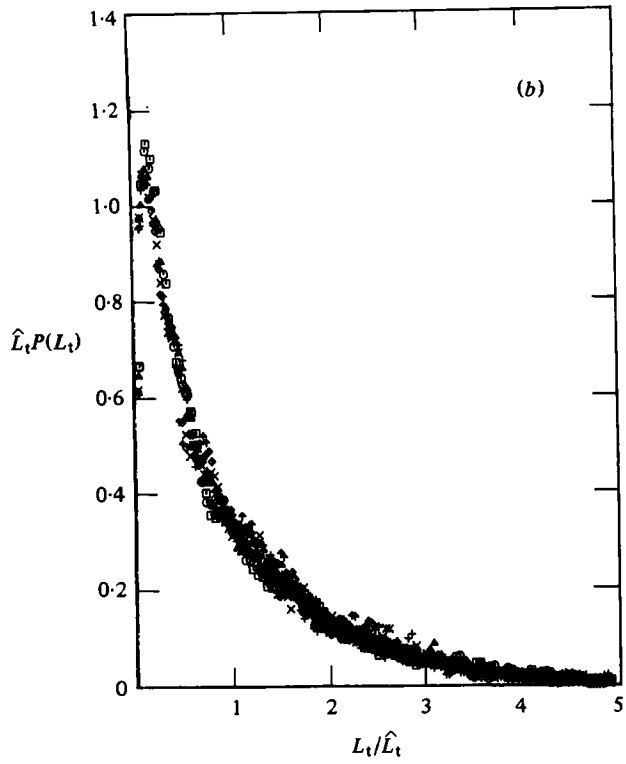

FIGURE 14. Collapse of conditional probability distribution of turbulent-zone length, $P(L_t|L_{min})$ (temperature scheme); short turbulent zones included, as in figure 13. $\gamma \approx 0{\cdot}5$. (*a*) $U_e\theta/\nu = 2430$. Values of L_{min}/δ: ⊡, 0·0179; ○, 0·0358; △, 0·0537; +, 0·0717; ×, 0·0896; ◇, 0·107; ⍋, 0·125. (*b*) $U_e\theta/\nu = 22000$ (data of Andreopoulos 1978). Values of L_{min}/δ: ⊡, 0·0167; ○, 0·033; △, 0·05; +, 0·067; ×, 0·0833; ◇, 0·1; ⍋, 0·169.

1000 boundary-layer thicknesses even at the highest Reynolds number. Some check processing was done with sample lengths of 11·3 s, with no effect on the shape of the p.d.f. except in the long tail. To remove some of the scatter from the tail the probability distributions were filtered with a rectangular window of width about $0{\cdot}1L$. Figure 15 shows the unconditional probability density functions for turbulent and irrotational zone lengths for $Re_\theta = 1100, 4820$ and (using Andreopoulos' data) 22000. The p.d.f. of turbulent-zone length falls from a peak value towards the origin, while the p.d.f. for irrotational-zone length peaks so close to the shortest interval recorded that it is by no means certain that it would in principle fall to the origin. Corrsin & Kistler argue that if the interface shape is differentiable there should be a negligible probability of bursts of length zero. This is not exactly true, as can be seen by considering a portion of the interface that has the shape of a Ω with the two legs touching; the curve is differentiable, but the turbulent-zone length measured at the point where the legs touch is zero. In practice, the shortest burst that can truly be called turbulent is of the order of the Kolmogorov scale. However, indefinitely short irrotational zones can occur in the fissures between two merging turbulent bursts (an interface configuration locally like a Y). The results of figure 15, and those of Chevray & Tutu (1978), qualitatively substantiate these arguments, and suggest that they hold at any Reynolds number. Figure 16 shows the Reynolds-number variation of the average turbulent and non-turbulent zone lengths. The strength of the variation with Reynolds number is remarkable, but ties up well with the general interpretation of

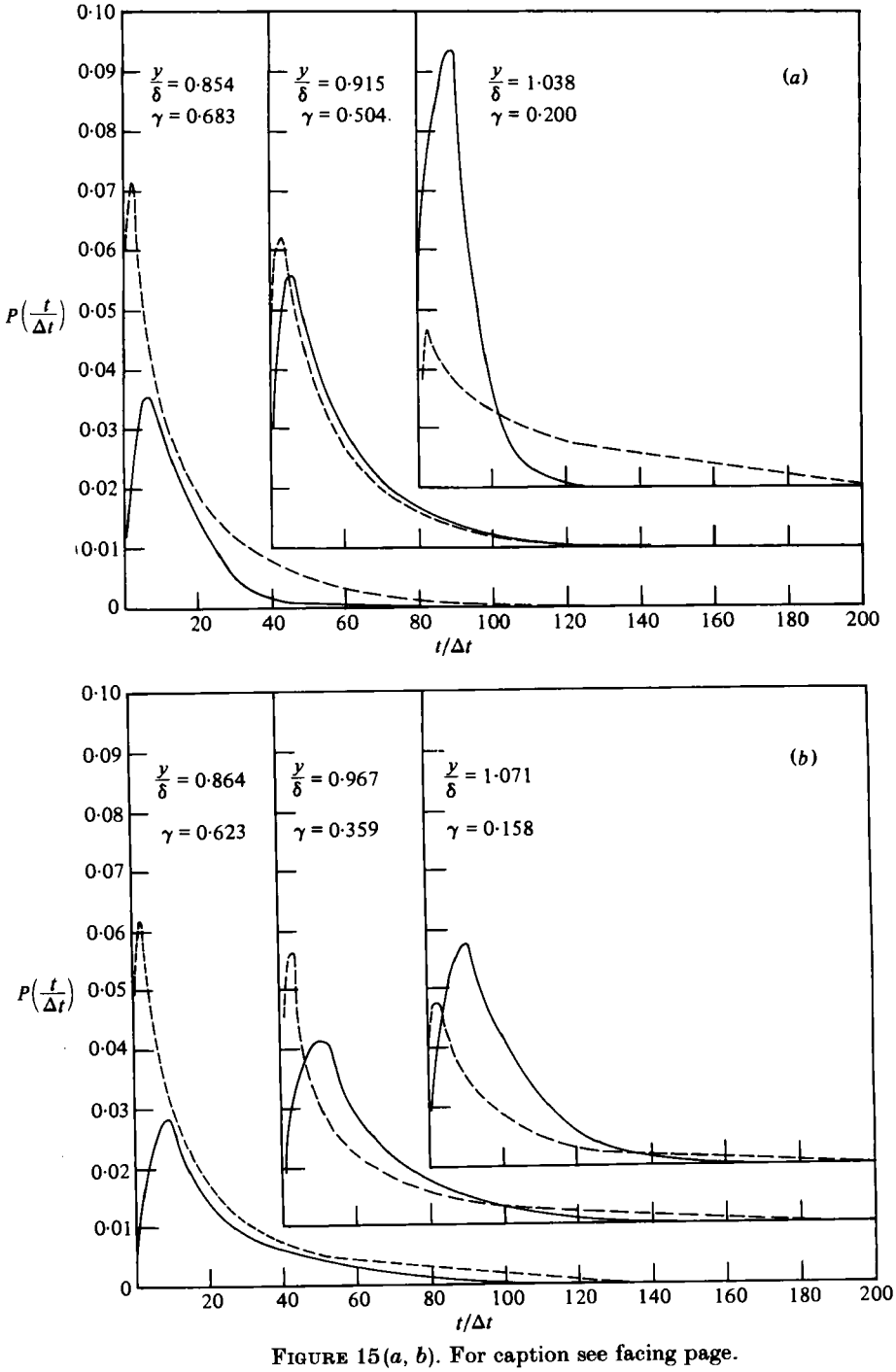

FIGURE 15(*a*, *b*). For caption see facing page.

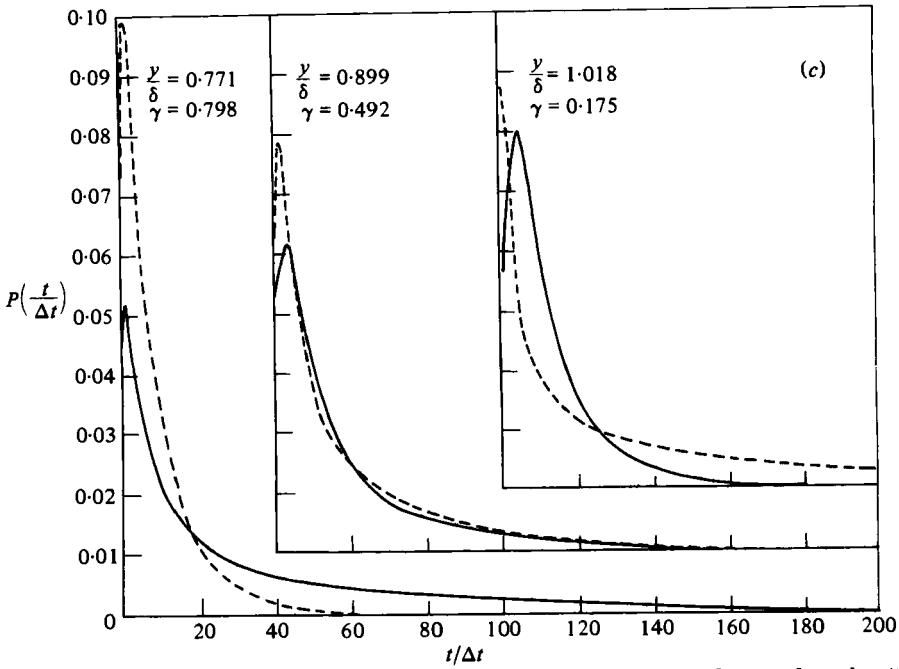

FIGURE 15. Probability distribution of turbulent and irrotational zone lengths (temperature scheme – zones of all lengths down to $3{\cdot}8 \times 10^{-4}\delta$ are included): ——, turbulent zone; – – – – – – irrotational zone. (*a*) $U_e\theta/\nu = 1100$. Values of y/δ and γ_θ are (left to right) 0·854, 0·683; 0·915, 0·504; 1·038, 0·200. (*b*) $U_e\theta/\nu = 4820$. Values of y/δ and γ_θ are (left to right) 0·864, 0·623; 0·967, 0·359; 1·071, 0·158. (*c*) $U_e\theta/\nu = 22000$. Values of y/δ and γ_θ are (left to right) 0·771, 0·798; 0·899, 0·492; 1·018, 0·175.

smoke pictures presented by Falco (1977), in which the 'typical-eddy' motion scaled on ν/u_τ so that the burst length becomes a small factor of δ as the Reynolds number increases. However, our average burst lengths tend to asymptote to constant values at high Reynolds number, of the same order as the $1{\cdot}6\delta$ (at $y/\delta = 0{\cdot}87$) quoted by Falco as the scale of the 'large-scale motion'. For the sake of comparison the wholesale and retail average turbulence-zone ('burst') lengths presented by Murlis (1975) using the velocity-intermittency scheme are shown in figure 17. The retail burst length, of course, is smaller by an order of magnitude than the wholesale burst length, but the latter is in tolerably good agreement with the burst length derived from the temperature-intermittency scheme. The value of $L_{\min}$ used in the wholesale burst processing was equal to 5 sampling intervals at all x-positions: since the Kolmogorov lengthscale η varies only as $\delta^{\frac{1}{4}}$ this is almost equivalent to a constant value of $L_{\min}/\eta$. It is interesting to note that both the wholesale burst length determined from the velocity-intermittency scheme and the burst length determined from the temperature-intermittency scheme decrease strongly with increasing y/δ, while the retail burst length, already small, does not fall so rapidly as y increases. Detailed differences between intermittency schemes over a range of Reynolds numbers are shown in figure 18, which compares probability distributions for the temperature-intermittency scheme and for the wholesale velocity-intermittency scheme with NMIN = 5. The correspondence of the two is quite good in the outermost part of the boundary layer, but poor at high intermittency, where the wholesale scheme seems to be least satisfactory in general.

The point at which the p.d.f. is a maximum indicates the 'most-probable' burst length, L_x say. The value of L_x deduced from the temperature intermittency statistics

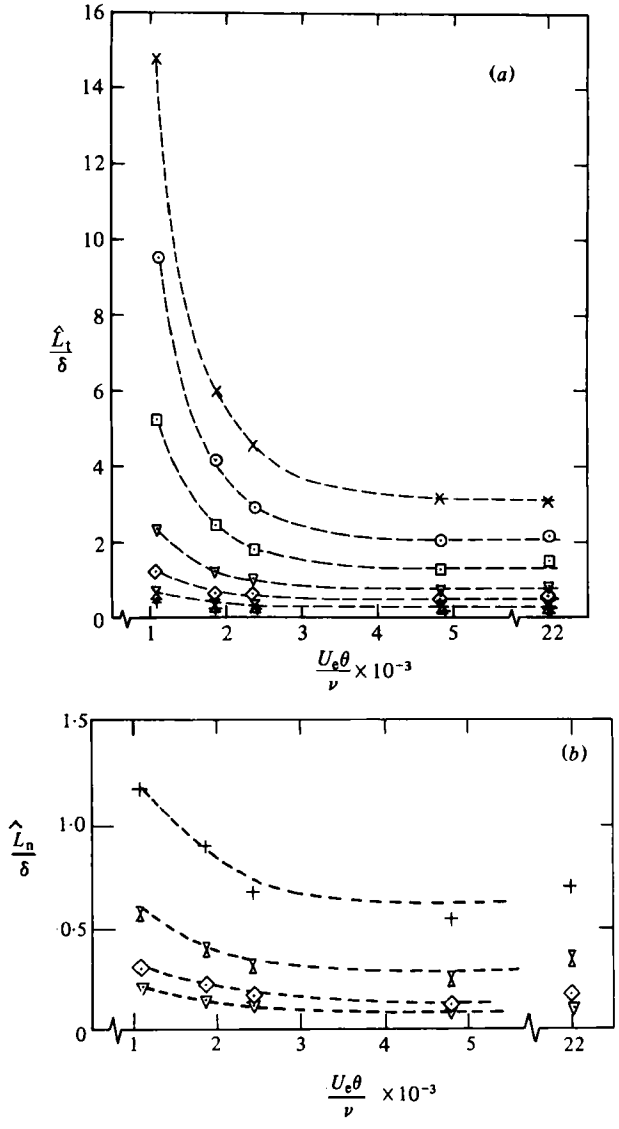

FIGURE 16. (*a*) Variation of average turbulent-zone length $\hat{L}_t$ with $U_e\theta/\nu$. Turbulence-biased temperature scheme. Values at $U_e\theta/\nu = 22000$ are from data of Andreopoulos (1978). ×, $y/\delta = 0{\cdot}4$, $\gamma = 0{\cdot}995$; ⊙, 0·5, 0·99; ⊡, 0·6, 0·955; ▽, 0·7, 0·89; ◇, 0·8, 0·77; ⧖, 0·9, 0·50; +, 1·0, 0·25. (*b*) Variation of average non-turbulent-zone length $\hat{L}_n$ with $U_e\theta/\nu$. Symbols as in (*a*).

is approximately independent of y, but decreases strongly with increasing Reynolds number. Figure 19 shows that L_x is very roughly half Falco's 'typical eddy' size c_x, and that $u_\tau L_x/\nu$ is rather accurately independent of Reynolds number and equal to about 120. The contribution of bursts of given length to the total intermittency is proportional to $LP(L)$, rather than to $P(L)$ itself, so that the interface shape is controlled mainly by bursts of length of order $\hat{L}$, the abscissa of the centroid of the p.d.f., rather than L_x. $\hat{L}$ is much larger than L_x and varies with y.

Figure 20 shows the turbulent burst *spacing* (reciprocal of number of bursts per unit length) made dimensionless with the local mean velocity and the boundary-layer thickness so that it equals (average burst spacing)/δ. Again a large variation with

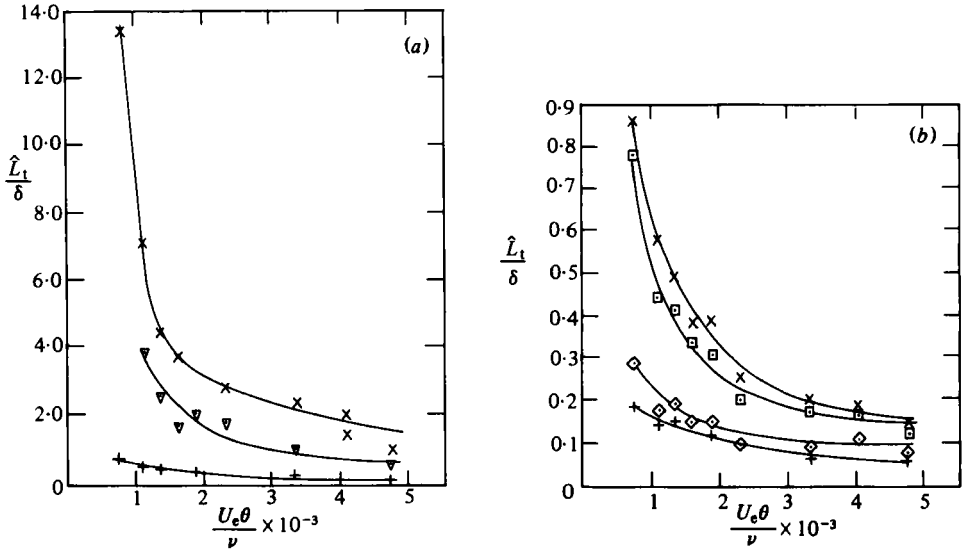

FIGURE 17. Variation of average turbulent-zone length $\hat{L}_t$ with $U_e\theta/\nu$. Velocity scheme. Symbols as in figure 16. (*a*) 'Wholesale' (turbulence-biased), NMIN = 5. (*b*) 'Retail'.

Reynolds number is seen, but in contrast to the burst length, which decreases monotonically as y increases, the burst spacing is a minimum near the point where $\gamma = 0{\cdot}5$. This is expected; burst frequency is zero outside the boundary layer, and also where $\gamma = 1$. Figure 21 is a cross-plot of figure 20, this time in terms of frequency, showing the trend with Reynolds number, and also showing that the dimensionless burst frequency becomes independent of Reynolds number at Reynolds numbers greater than about 5000, as in the case of the burst length.

Although probability distributions and their miscellaneous statistics are less easy to understand by inspection than a smoke picture, it is clear from the discussion above that the present results are compatible with, and extend, the smoke studies and associated hot-wire measurements made by Falco (1980) and Head & Bandyopadhyay (1981) (hereinafter cited as RF and HB respectively). Perhaps our most important result, shown in figures 16 and 21, is that the dominant lengthscales of the interface become independent of Reynolds number at $Re_\theta \approx 5000$, like the wake parameter Π shown in figure 2. This behaviour of the lengthscale implies that RF's 'typical eddies' and HB's 'hairpin vortices', which are, clearly, different observers' views of the same phenomenon and which, like the superlayer thickness, scale on the viscous length ν/u_τ, do not have a significant effect on the main features of interface shape at high Reynolds numbers. Of course the 'typical eddies' are still expected to dominate the *smallest*-scale corrugations of the interface – that is, the viscous superlayer itself. However the Reynolds-number independence of interface lengthscale and Π rescues the traditional model of viscosity-independent 'large eddies', which control the dominant lengthscales of the interface and the shear-stress production. At low Reynolds numbers the typical eddies are no longer small compared with the boundary-layer thickness ($c_x/\delta = 0{\cdot}1$ at $Re_\theta = 6000$ and $1{\cdot}0$ at $Re_\theta = 400$), and will affect the shear-stress production, both directly and via their effect on the large eddies. Falco (1977) noted that at $Re_\theta \approx 1000$ the large eddies still have a definable flow field although the typical eddies contribute effectively the whole of the Reynolds stress in the outer region. A referee has discussed the possible scenarios for large-eddy/typical-eddy interaction: if one discounts Townsend's (1956) original idea

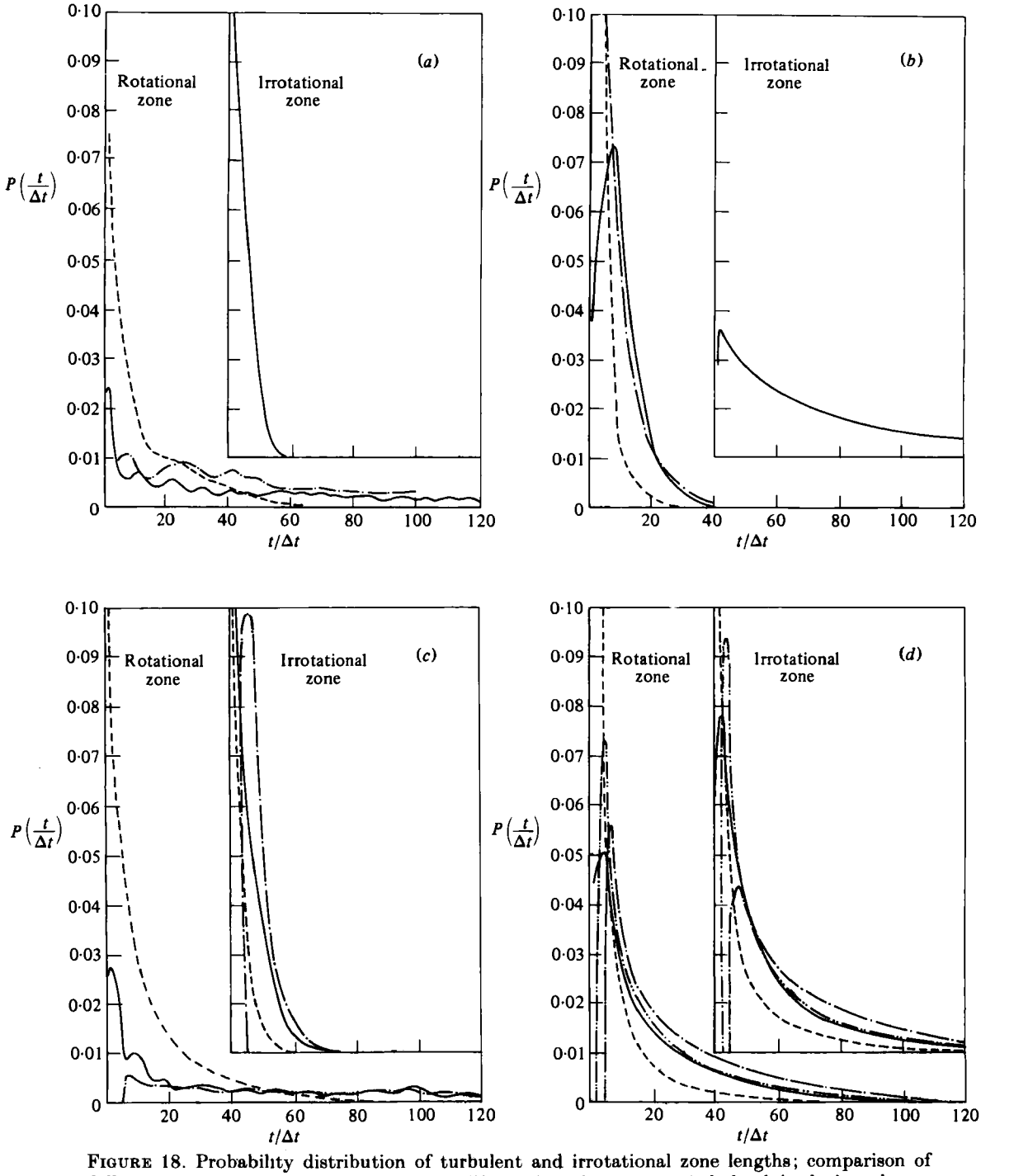

FIGURE 18. Probability distribution of turbulent and irrotational zone lengths; comparison of different intermittency schemes: ——, 'retail' velocity scheme; –·–·, 'wholesale' velocity scheme, NMIN = 5; –··–··, 'wholesale' velocity scheme NMIN = 2; ——, temperature scheme. (*a*) $U_e\theta/\nu = 1100$, $y/\delta \approx 0{\cdot}4$; (*b*) 1100, 1·0; (*c*) 22000, 0·48; (*d*) 22000, 0·90.

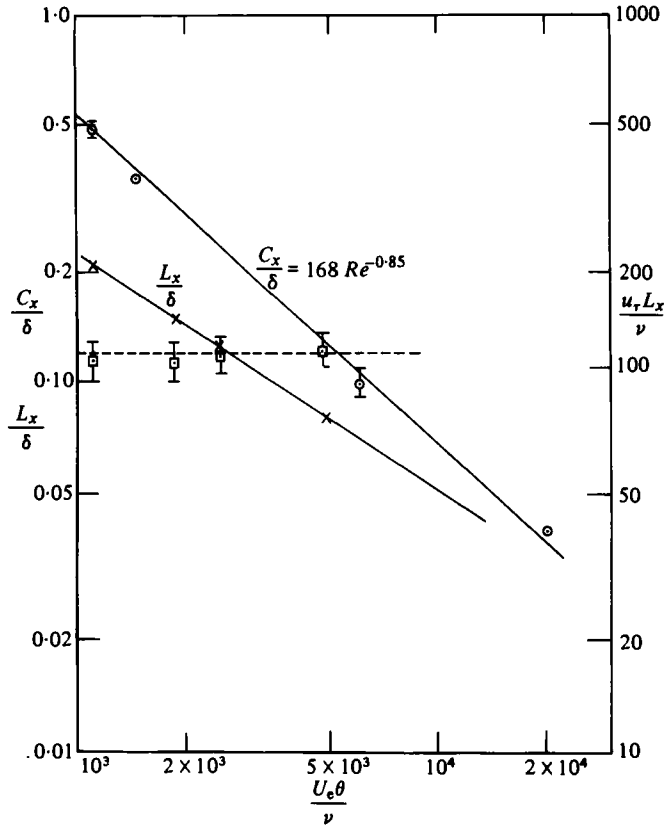

FIGURE 19. Variation of most-probable turbulent-zone length L_x (i.e. value of L_t for maximum $P(L_t)$) with $U_e\theta/\nu$, compared with 'typical-eddy' size C_x (Falco 1974, quoted by Willmarth 1975). Note: L_x is independent of y in the outer-layer region. ×, L_x/δ; ⊡, $u_\tau L_x/\nu$; ⊙, C_x/δ.

that the large eddies control interface statistics but do not generate significant Reynolds stress, the only choice that fits all the data is that – in the referee's words – 'the large eddies are weak at low Reynolds numbers, where the momentum transport is accomplished by both "typical eddies" and the large-scale motions, and as Reynolds number increases, the contributions of the "typical eddies" decreases while that of the large scale motions increases.' Our results, however, suggest that the large eddies are still influential at low Reynolds numbers.

The 'typical eddies'/'hairpin vortices' seen in smoke pictures are exceptionally well-organized structures – it is easy to see that a hairpin or horseshoe is the shape assumed by a perturbed spanwise vortex line in a mean shear field – and the increase in mixing length found at low Reynolds numbers is evidently a consequence of this (although, curiously, the shear-correlation coefficient, another traditional measure of organization, does not vary significantly with Reynolds number). The large eddies also are often claimed to be horseshoe-like, and the large-eddy model of Townsend (1976, p. 120) based on the results of Grant (1958) is reminiscent of the two legs of a hairpin vortex without the transverse vortex joining them. However the dynamic process or 'instability' that produces typical eddies is limited by viscosity, while the production of large eddies is not, so a close correspondence cannot be expected. HB's comment, that the large eddies at $Re_\theta > 2000$ appear to be made up of random agglomerations of hairpins, cannot be rigorously inferred from their pictures of

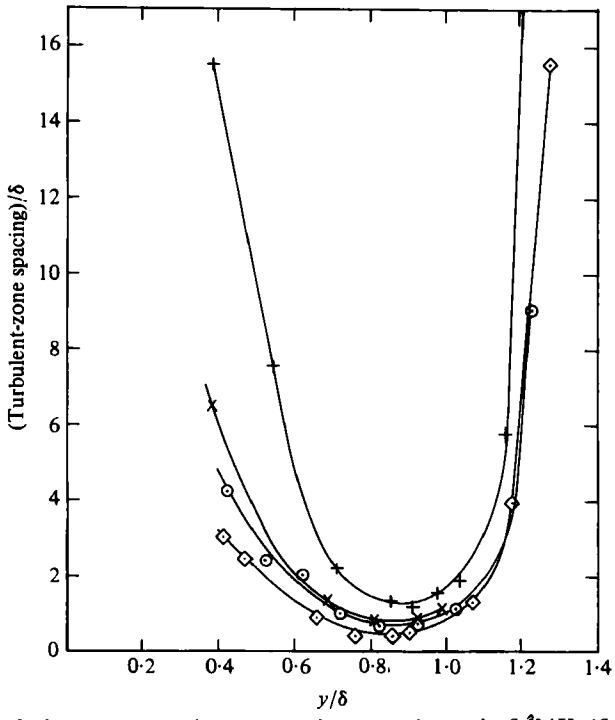

FIGURE 20. Turbulent-zone spacing (approximate reciprocal of $f\delta/U_e$ if $U \approx U_e$). Values of $U_e\theta/\nu$: +, 1100; ×, 1880; ⊙, 2430; ◇, 4820.

smoke-filled boundary layers, which, by definition, show only the interface. Motions like the superlayer typical eddies can be seen within the turbulence, but this probably reflects the universality of viscosity-limited vortex dynamics rather than a common origin for the superlayer eddies and the internal eddies.

The above results, though quantitative in nature and providing a useful alternative to the inevitably subjective interpretation of smoke pictures, are mainly qualitative in *use*. They support the Huffman & Bradshaw hypothesis that low-Reynolds-number effects reside in the superlayer, and provide a framework for the interpretation of the turbulence measurements to be presented below.

3.4. *Turbulence measurements*

Turbulence-intensity profiles at different Reynolds numbers are shown in figure 22, and it is seen that the agreement between the present results at the highest Reynolds number, $Re_\theta = 4750$, and the measurements of Klebanoff (1955) at $Re_\theta = 8000$ is good, except in the outer region, where the present values of $\overline{u^2}$ seem to be somewhat larger than Klebanoff's. However, as mentioned above, it is difficult to extract the correct value of δ for scaling Klebanoff's results. A strong dependence on Reynolds number of the $\overline{u^2}$ profiles, and to a lesser extent the $\overline{v^2}$ profiles, can be seen. The conditionally sampled averages, expressed as their contributions to overall means, are shown in figure 23. Turbulent zones make an overwhelming contribution to overall averages, with irrotational zones contributing only about $0{\cdot}01u_\tau^2$ to the wholesale averages (not shown here) and $0{\cdot}05u_\tau^2$ to the retail averages. Figure 24 shows $\overline{u^2}/\overline{v^2}$, which increases strongly with Re. The streamwise variations of u- and v-component intensities at fixed values of y/δ are shown in figures 25 and 26. Shear stress (figure 27) shows a somewhat smaller variation with Reynolds number than that inferred by Green (1971) from mean-velocity profile measurements.

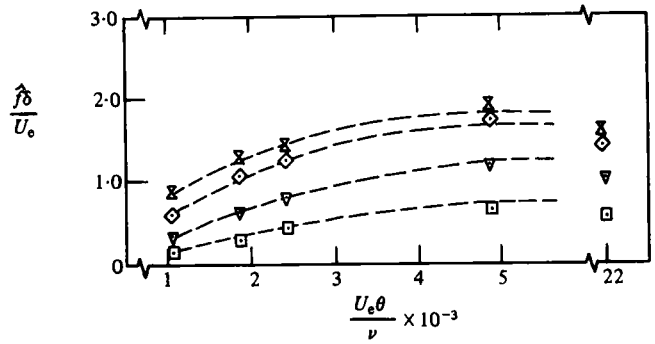

FIGURE 21. Variations of turbulent-zone frequency $\hat{f}$ with $U_e\theta/\nu$: ⊡, $y/\delta = 0{\cdot}6$, $\gamma = 0{\cdot}955$; ▽, 0·7, 0·890; ◇, 0·8, 0·77; ⧖, 0·9, 0·50.

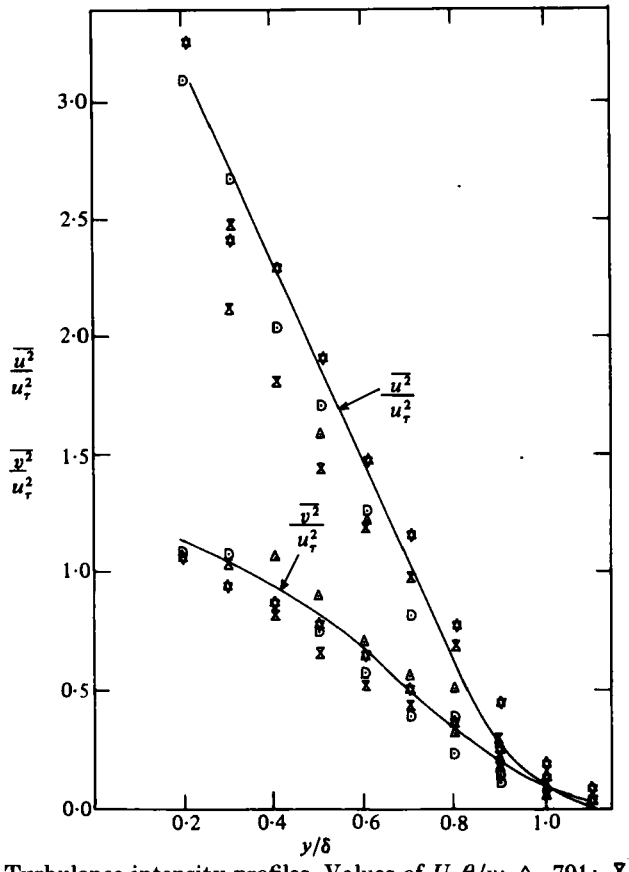

FIGURE 22. Turbulence-intensity profiles. Values of $U_e\theta/\nu$: △, 791; ⧖, 1368; ⊡, 3362; ✡, 4750. ——, Klebanoff (1955), $U_e\theta/\nu \approx 8000$.

The best measure of structural changes is the behaviour of the dimensionless parameter $\overline{u^2}/\overline{v^2}$ and the shear correlation coefficient $-\overline{uv}\,(\overline{u^2}\,\overline{v^2})^{-\frac{1}{2}}$. As seen in figure 24, the intensity ratio at high Reynolds number follows Klebanoff's measurements fairly well (our $\overline{v^2}$ is a little lower than Klebanoff's) but at low Reynolds number $\overline{u^2}/\overline{v^2}$ is generally smaller, rising to a roughly constant value by about $Re_\theta = 2000$. Data for the shear-correlation coefficient R_{12} at different y/δ plotted in figure 28, on displaced axes for clarity, show a peak at about $Re_\theta = 1900$ followed by a slow fall to a nearly asymptotic value at $Re_\theta = 4750$. Values of R_{12} at $y/\delta = 0{\cdot}6$ are $-0{\cdot}42$ at

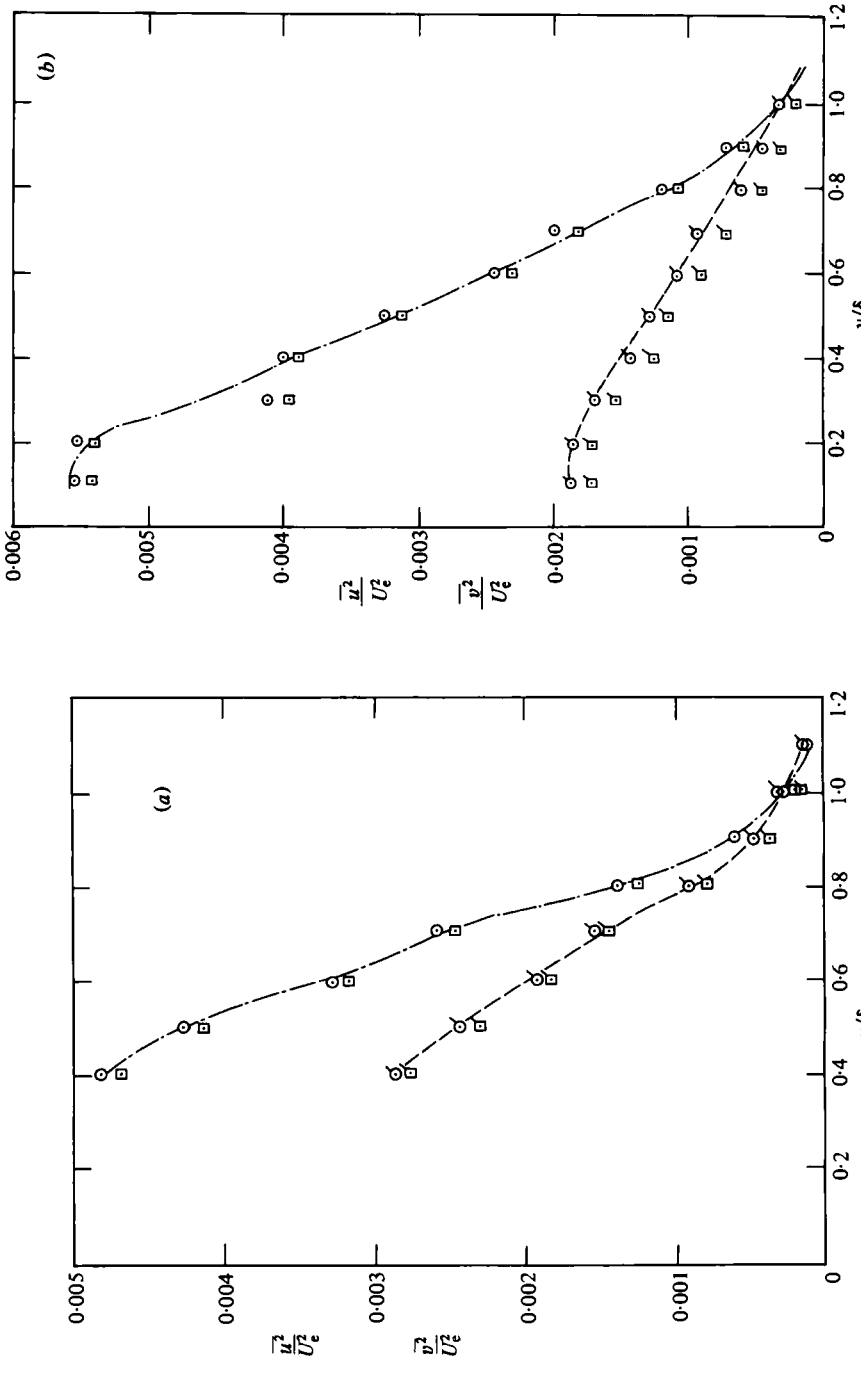

FIGURE 23. Conventional and conditional turbulent intensities. ⊙, $\overline{u^2}$; □, $\gamma_u \overline{u^2}_{\mathrm{RE}}$; ⊙, $\overline{v^2}$; □, $\gamma_u \overline{v^2}_{\mathrm{RE}}$.
(*a*) $U_e\theta/\nu = 791$; (*b*) $U_e\theta/\nu = 4750$.

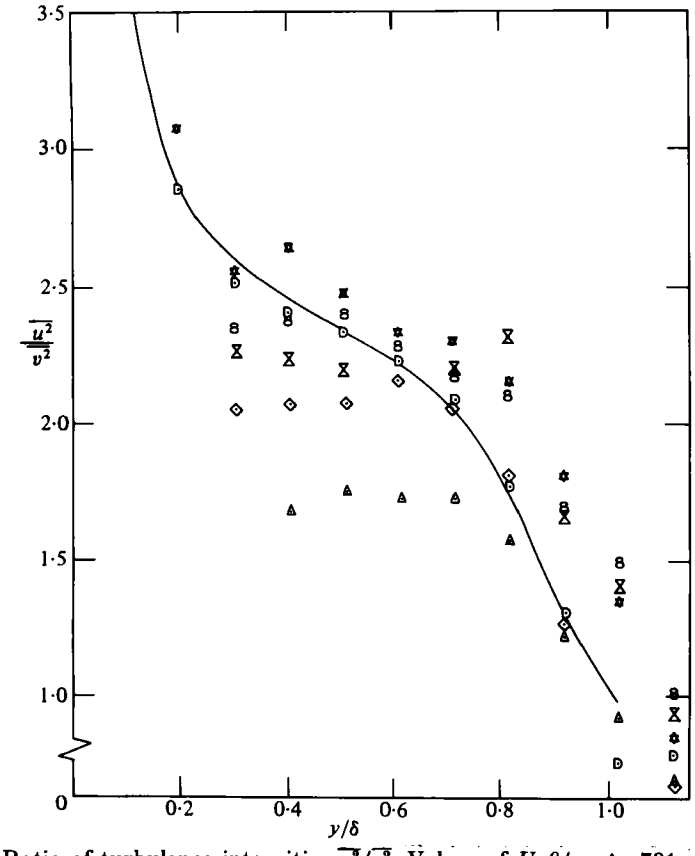

FIGURE 24. Ratio of turbulence intensities $\overline{u^2}/\overline{v^2}$. Values of $U_e\theta/\nu$: △, 791; ◇, 1112; ⧖, 1368; 8, 1900; D, 3362, ✡, 4750. ——, Klebanoff (1955), $U_e\theta/\nu \approx 8000$.

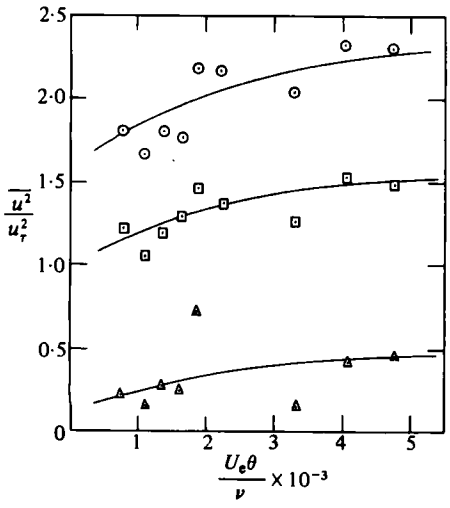

FIGURE 25.

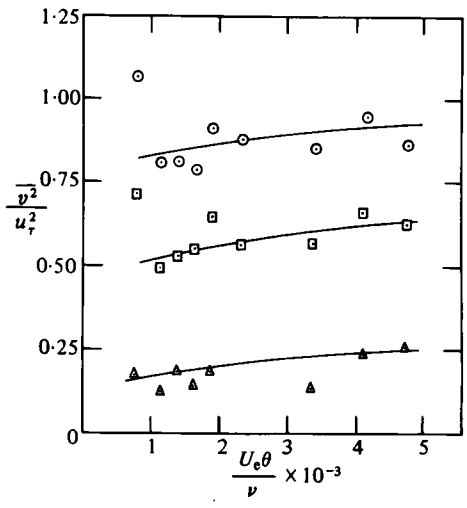

FIGURE 26

FIGURE 25. Variation of u-component intensity with $U_e\theta/\nu$: ⊙, $y/\delta = 0{\cdot}4$; ⊡, 0·6; △, 0·9.

FIGURE 26. Variation of v-component intensity with $U_e\theta/\nu$: ⊙, $y/\delta = 0{\cdot}4$; ⊡, 0·6; △, 0·9.

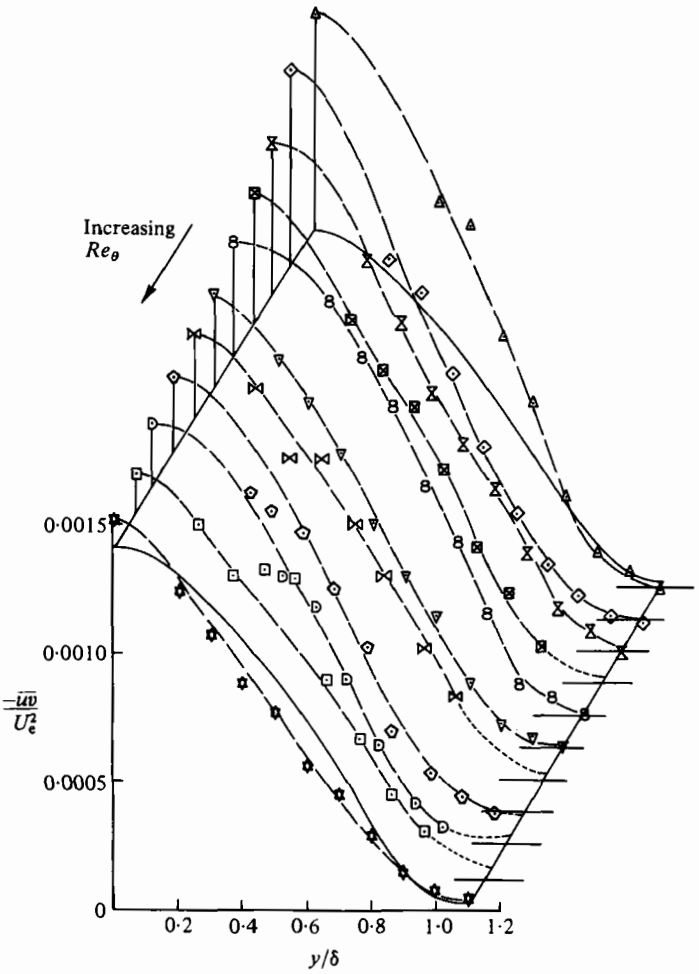

FIGURE 27. Shear-stress profiles, normalized by U_e. Values of $U_e\theta/\nu$: △, 791; ◇, 1112; ⧖, 1368; ⊠, 1640, ⊗, 1900; ▽, 2192; ⋈, 2387; ⬠, 2620; ▷, 3362; ⊡, 4108; ✡, 4750. ——, Klebanoff (1955), $U_e\theta/\nu \approx 8000$.

$Re_\theta = 791$, $-0{\cdot}45$ at $Re_\theta = 1900$, and $-0{\cdot}40$ at $Re_\theta = 4750$. The difference in the streamwise development of R_{12} and $\overline{u^2}/\overline{v^2}$ is somewhat perplexing. The shear-correlation coefficient is probably the better measure of the efficiency of turbulent mixing, and it is plausible that this should reach a maximum at a Reynolds number intermediate between that at which the turbulence is altogether damped out by viscosity and a Reynolds number at which a locally isotropic region of the wavenumber spectrum, contributing to the intensities but not to the shear stress, begins to be important. $\overline{v^2}/\overline{u^2}$ is also a crude measure of the efficiency of turbulent mixing, or, more strictly, of the coherence of the turbulent eddies; it is well known that almost any turbulent eddy will contribute to the longitudinal-component velocity fluctuation u, because of the presence of a mean-velocity gradient dU/dy, while v-component motions are more likely to be associated with the sort of erupting eddies that effect most of the turbulent mixing. Thus the monotonic increase in $\overline{u^2}/\overline{v^2}$ implies a monotonic decrease in the general efficiency of turbulent mixing. Whatever the qualitative explanation, the quantitative results show large variations of eddy

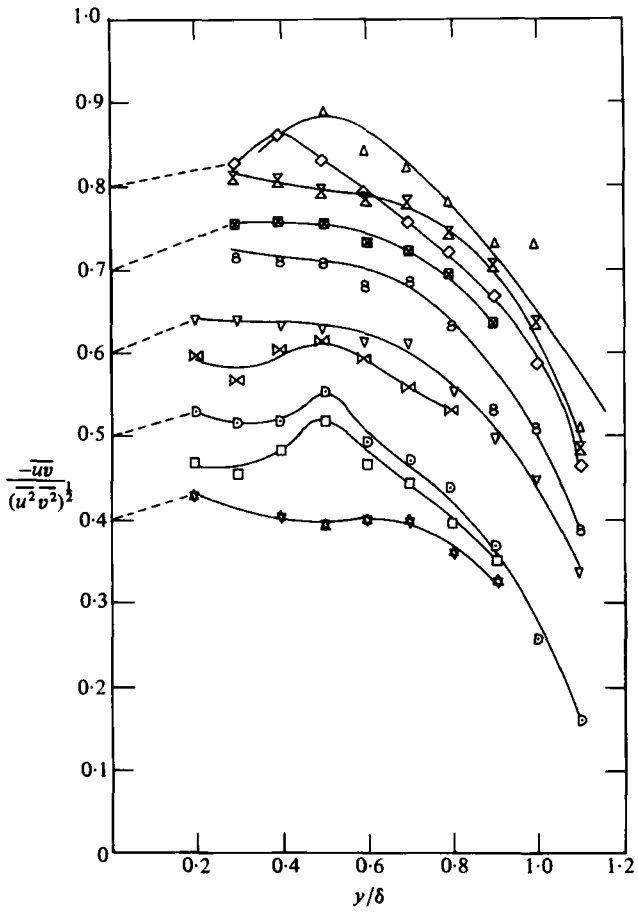

FIGURE 28. Shear-correlation coefficient $R_{12} \equiv \overline{uv}(\overline{u^2}\overline{v^2})^{-\frac{1}{2}}$. Symbols as in figure 27. Ordinate scale is for $U_e\theta/\nu = 4750$. Other curves are successively displaced by 0·05 units: dotted lines point to 0·40 on relevant scale.

structure with Reynolds number. Finally, the importance of vortices inclined at 45° to the flow direction, identified by HB, is measured by

$$\frac{\overline{(u-v)^2}}{\overline{(u+v)^2}} \equiv \frac{r^2-2R_{12}r+1}{r^2+2R_{12}r+1},$$

where $r^2 \equiv \overline{u^2}/\overline{v^2}$. Values at $Re_\theta = 791$, 1900, 4750 are 2·35, 2·40, 2·16, following the behaviour of R_{12} rather than $\overline{u^2}/\overline{v^2}$.

Turbulent energy balances at two different stations are shown in figure 29, normalized with the local boundary-layer thickness but with the free-stream velocity rather than the rapidly varying local friction velocity (results at the lowest Re are not given because of the difficulty of evaluating streamwise derivatives at the end of the range). The most noticeable feature is the smallness of the advection at low Reynolds number: at high Reynolds number, advection and diffusion are nearly equal and opposite in the outer layer. The reason is that, although the boundary layer is growing rapidly, typical intensity levels are decreasing with increasing Reynolds number, following the trend in c_f. Diffusion, on the other hand, is fairly strong at low Reynolds numbers, the point at which diffusion equals production being about $y/\delta = 0{\cdot}72$ at $Re_\theta = 800$ compared with $y/\delta = 0{\cdot}82$ at $Re_\theta = 4750$ (as usual the

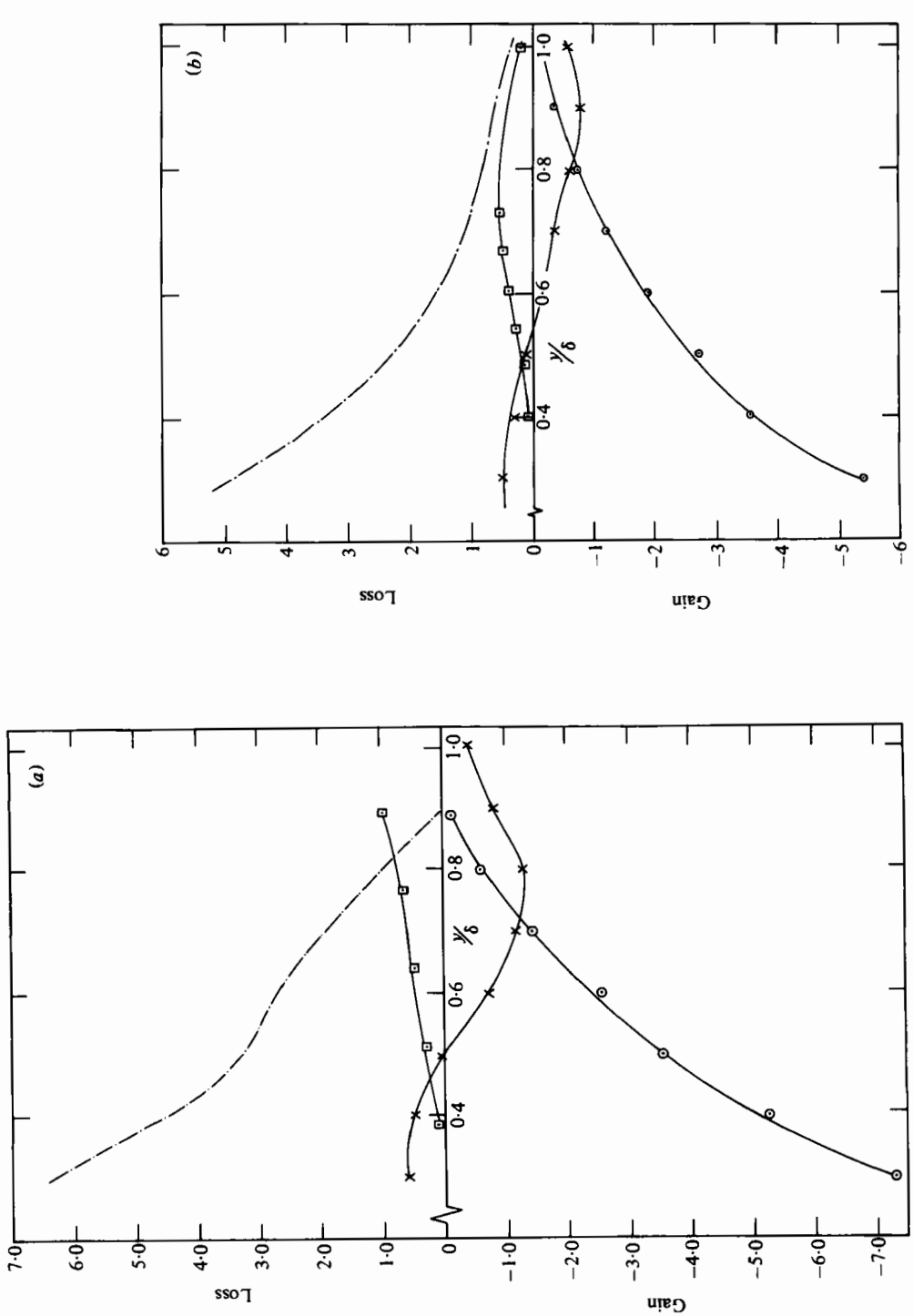

FIGURE 29. Turbulent-energy balance, normalized by δ/U_e^3. ○, production $-\overline{uv}\partial U/\partial y$; ⊡, advection $D\frac{1}{2}(\overline{u^2}+\overline{v^2}+\overline{w^2})/Dt \approx D\frac{1}{2}(\overline{u^2}+\overline{v_2})/Dt$; ×, diffusion $\partial(\overline{p'v}/\rho+0{\cdot}5\overline{(u^2+v^2+w^2)v})/\partial y \approx \partial[0{\cdot}75(\overline{u^2}+\overline{v^2})\overline{v}]/\partial y$; ———, dissipation, by difference. (a) $U_e\theta/\nu = 1112$; (b) $U_e\theta/\nu = 4750$.

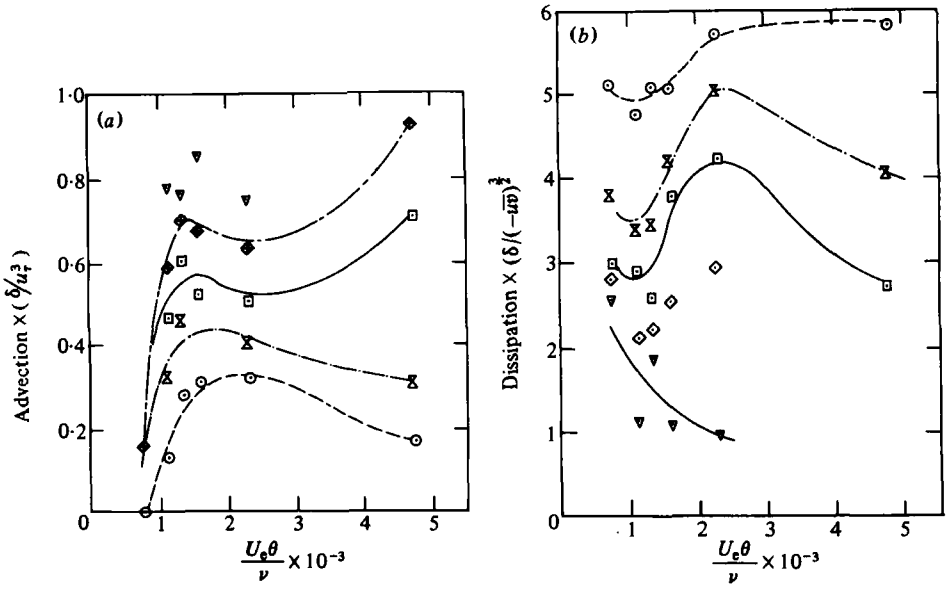

FIGURE 30. Variation of energy-balance terms, normalized by δ/u_τ^3, with $U_e\theta/\nu$. ——⊙—, $y/\delta = 0{\cdot}4$; —— ⧖ ——, 0·5; ——⊡——, 0·6; ◇, 0·7; ▽, 0·8. (*a*) advection; (*b*) dissipation, ϵ; $\epsilon\delta/(-\overline{uv})^{\frac{3}{2}} \equiv \delta/L_\epsilon$, where L_ϵ is the dissipation-length parameter.

contribution of the pressure-fluctuation term to the diffusion, being unmeasurable, has been ignored; also, the dissipation has been obtained by difference from the other terms).

Figure 30 shows the streamwise development of the different terms in the turbulent energy equation. Production (not shown), normalized by the *friction velocity* and the total boundary-layer thickness, increases with increasing Reynolds number as the normalized velocity gradient $(\delta/u_\tau)\,dU/dy$ in the outer layer increases owing to the increase in wake component. Advection, as already remarked, increases significantly with Reynolds number while diffusion decreases. Dissipation values have been plotted normalized by the value of shear stress at the same point, rather than by u_τ, so that $\epsilon\delta(\tau/\rho)^{-\frac{3}{2}} \equiv \delta/L_\epsilon$, where L_ϵ is the 'dissipation' length parameter. There seems to be a general increase with Reynolds number: the results, especially those from the last station (requiring a differentiation at the end of the range to obtain the advection), are not very reliable. The results imply a decrease in L_ϵ/δ with increasing Reynolds number, which corresponds qualitatively to the increase in lengthscale or mixing length normally found necessary to obtain good predictions of low-Reynolds-number boundary layers.

The shear-stress balances at different Reynolds numbers are presented by Murlis (1975); the plots will not be reproduced here. Again, the mean-flow transport term (corresponding to the advection in the turbulent energy equation) is very much smaller at low Reynolds numbers than at the last station, while the turbulent transport is – again – very much larger at low Reynolds numbers than at high Reynolds numbers. An interesting feature of shear stress is that, at the lowest Reynolds number, the turbulent transport in the inner part of the layer ($y/\delta < 0{\cdot}4$) is fairly small, rises to a peak at an intermediate Reynolds number and then falls to perhaps half this peak value at the highest Reynolds number.

The detailed behaviour of the turbulent transport of turbulent energy and of shear stress is best discussed by direct reference to the triple products, rather than to their

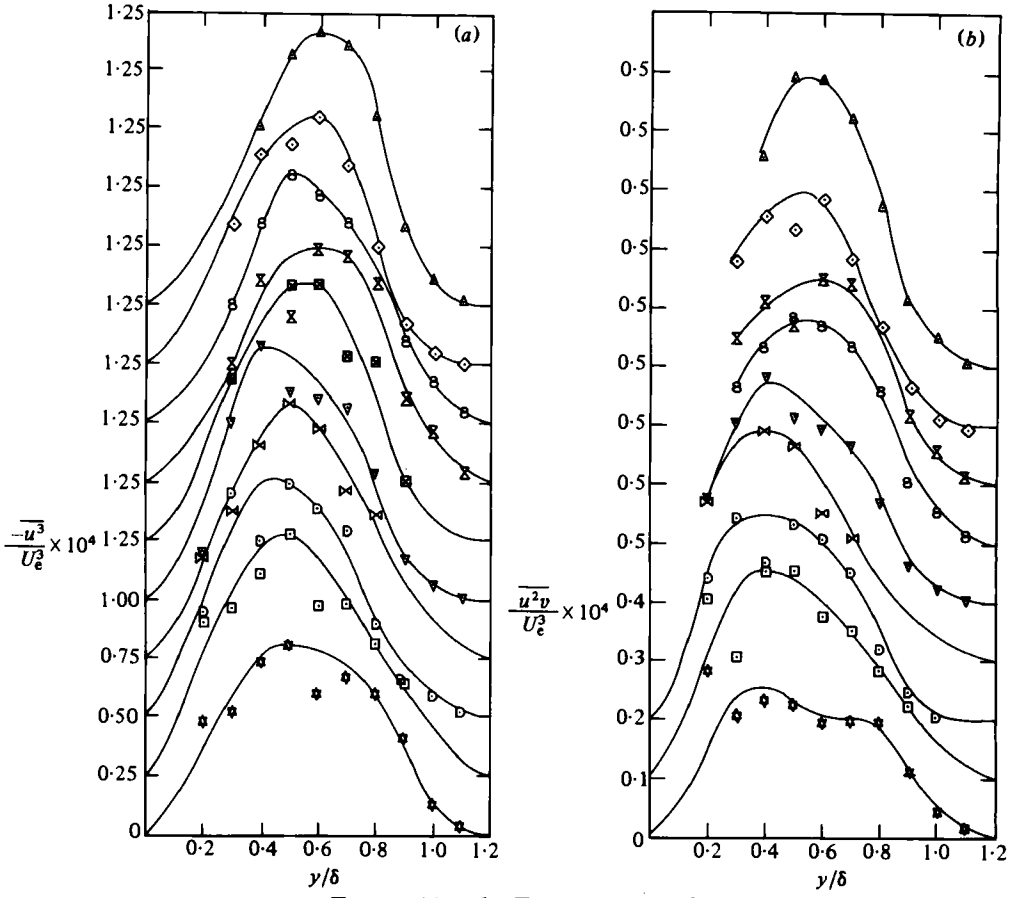

FIGURE 31 (*a*, *b*). For caption see facing page.

gradients which appear in the transport equations. Figures 31 (*a*)–(*d*) show the present results at different Reynolds numbers. Figure 32 compares the present results at the highest Reynolds number with those of other workers as available. As is well known, triple products do not scale exactly on u_τ^3, so that no simple plot would collapse all the results, but the comparison with the results of Andreopoulos (1978; *smooth* surface) with 0·7 times the u_τ^3 is acceptably good. Hedley & Keffer's (1974*b*) results are also shown, but here discrepancies in shape appear: Hedley & Keffer say that their artificially thickened boundary layer may not have been in equilibrium, and this could affect the outer-layer results, but their inner-layer results also seem implausible. As in the case of the second-order products, the irrotational-zone contributions are fairly small and will be ignored in the present discussions. However, the different sets of results agree fairly well in the outer part of the boundary layer, which is the region of main interest in the present discussion. The present results (figure 31) show that in all cases the maximum value decreases with increasing Reynolds number while the position of the maximum value moves towards the surface. Figure 33 shows the streamwise variation of the different triple products, normalized with the local friction velocity in each case. The results are somewhat scattered but, with the exception of $\overline{u^3}$, the general tendency is for a small peak to appear at $u_e\theta/\nu \approx 3000$. Compared with the rather spectacular changes in the second-order anisotropy parameters, the variation of the triple products in this

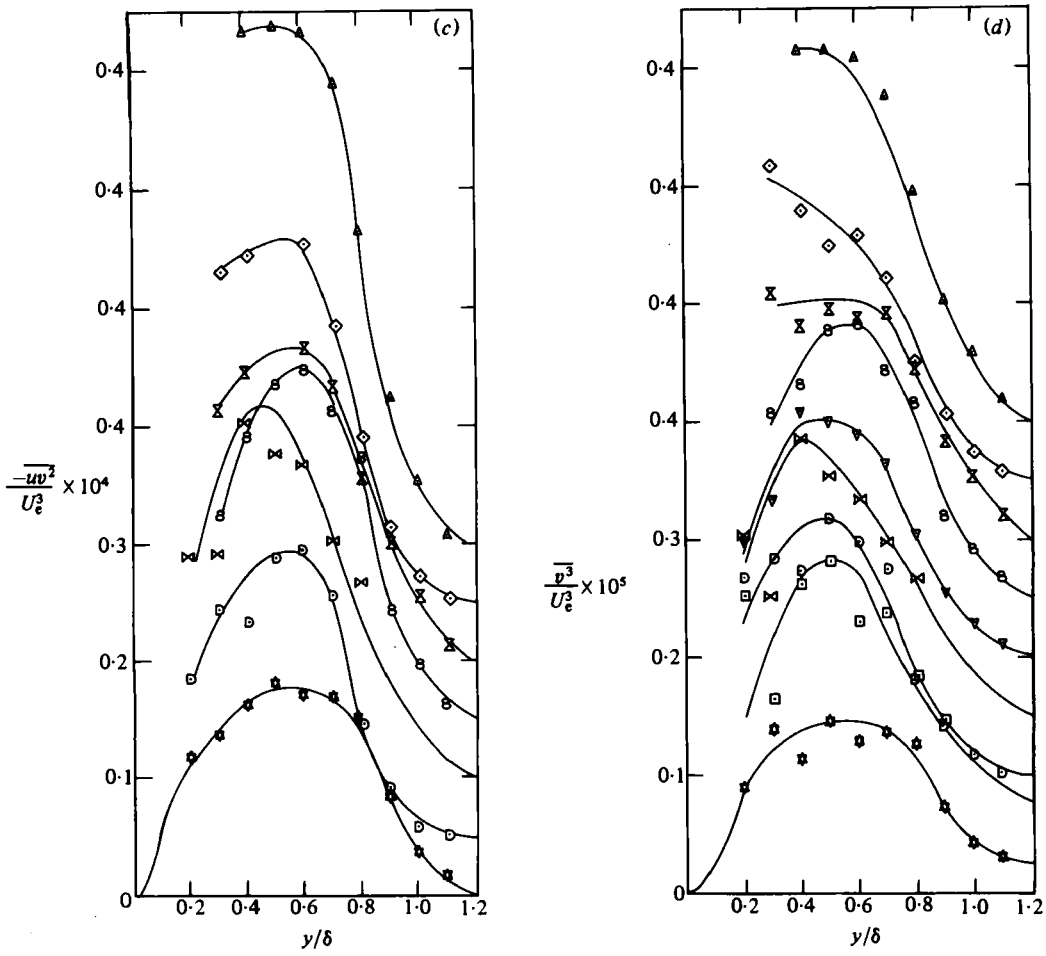

FIGURE 31. Triple products, normalized by U_e^3. Values of $U_e\theta/\nu$: △, 791; ◇, 1112; 8, 1368; ⧖, 1640; ⊠, 1900; ▽, 2192; ⋈, 2387; ▷, 3362; ⊡, 4108; ✡, 4750. (*a*) $-\overline{u^3}$: ordinate scale is for $U_e\theta/\nu = 4750$; other curves successively displaced by 0·25 units. (*b*) $\overline{u^2v}$; ordinate scale is for $U_e\theta/\nu = 4750$; other curves successively displaced by 0·1 units. (*c*) $-\overline{uv^2}$; ordinate scale is for $U_e\theta/\nu = 4750$; other curves successively displaced by 0·05 units. (*d*) $\overline{v^3}$; ordinate scale is for $U_e\theta/\nu = 4750$; other curves successively displaced by 0·05 units.

dimensionless form is fairly small, especially in the case of the shear-stress transport $\overline{uv^2}$. This suggests that the basic turbulent-transport mechanisms for turbulent energy and shear stress do not change qualitatively with Reynolds number. If one accepts that the main contribution at high Reynolds number comes from the large eddies (Falco's 'large-scale motions'), the simplest inference from this and the preceding result is (i) that the large eddies are still present, although somewhat weakened, at low Reynolds number, and (ii) that the 'typical eddies' in the superlayer do not effect much turbulent transport of Reynolds stress even at low Reynolds number, although they contribute significantly to momentum transport. The alternative is to suppose that both types of eddies contribute to turbulent transport, but that the large-scale motions take over from the very dissimilar typical eddies in such a way that third-order structural parameters change comparatively little as the Reynolds number increases, and this seems an unlikely coincidence. This implies that, at least if triple products are related to local values of shear stress rather than to shear-stress gradient, the

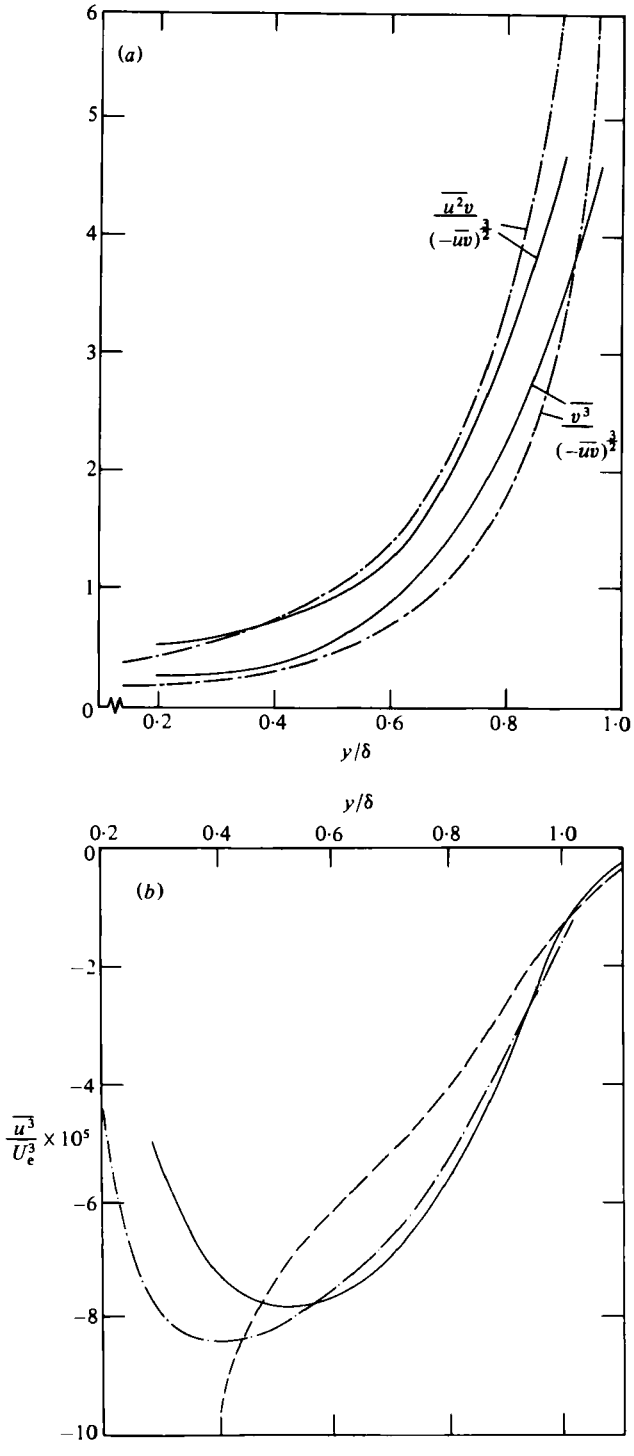

FIGURE 32. Triple products: ——, present results $U_e\theta/\nu = 4750$; – – – –, Hedley & Keffer (1974*b*), $U_e\theta/\nu = 9700$; —·—·—, Andreopoulos (1978), $U_e\theta/\nu = 13600$ (*smooth* surface). (*a*) $\overline{u^2v}$ and $\overline{v^3}$, normalized by $-\overline{uv}$; (*b*) $\overline{u^3}$; (*c*) $\overline{v^3}$; (*d*) $\overline{uv^2}$; (*e*) $\overline{u^2v}$.

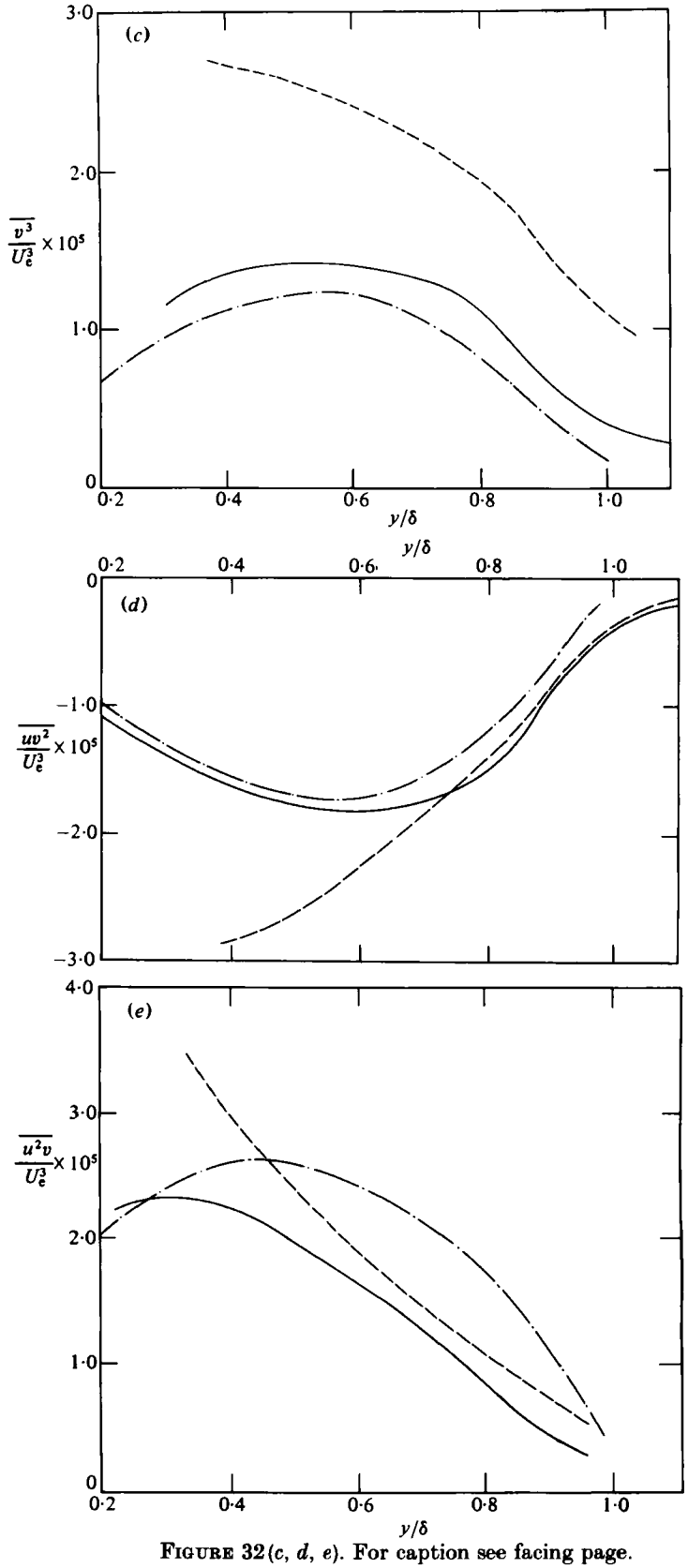

FIGURE 32(*c*, *d*, *e*). For caption see facing page.

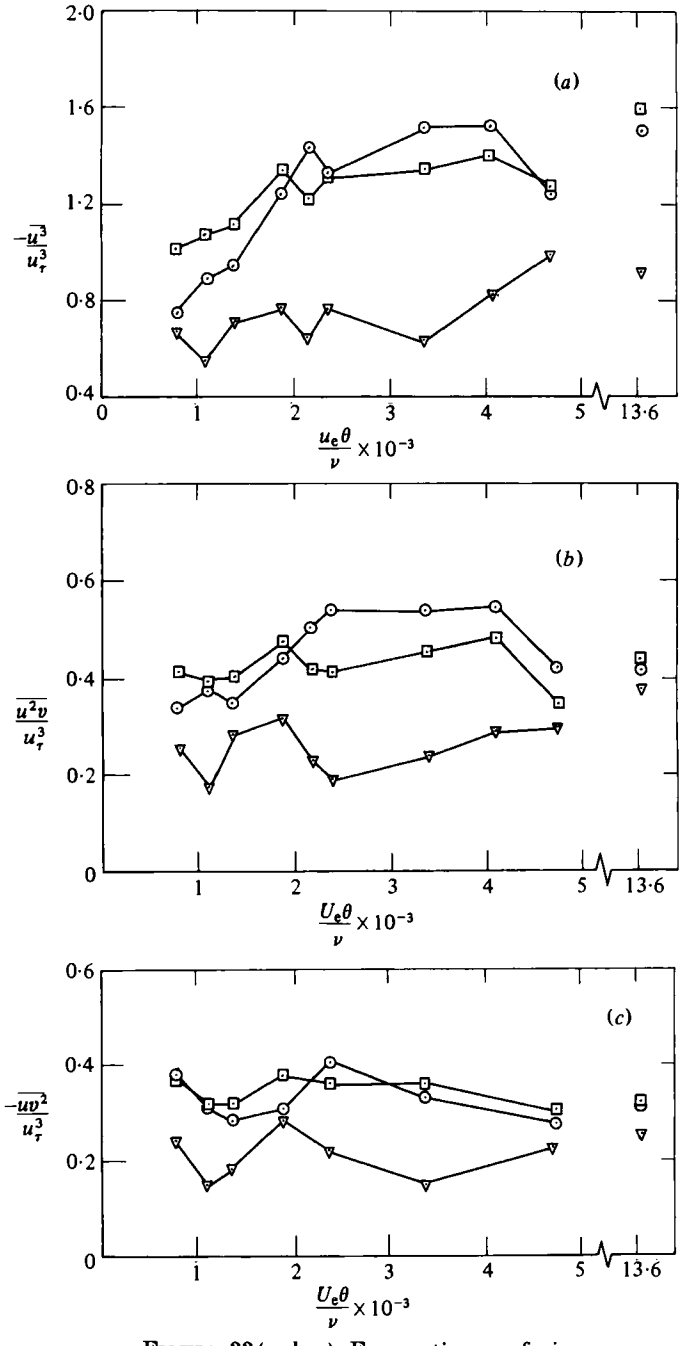

FIGURE 33(*a*, *b*, *c*). For caption see facing page.

turbulent-transport assumptions made in calculation methods should not need significant adjustment for local Reynolds-number effects.

Further details and analysis of triple and quadruple velocity products are given by Murlis (1975); scales in his figure 5.4.12 are incorrect (figures 5.4.1–5.4.9 are correct).

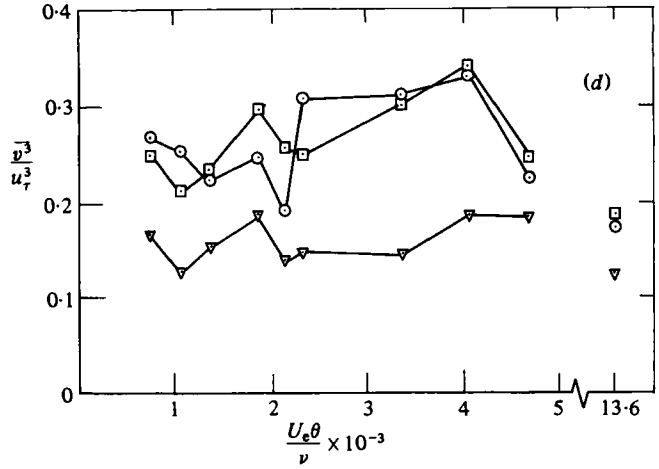

FIGURE 33. Variation of triple products, normalized by u_τ^3, with $U_e\theta/\nu$. Note false origins. Values at $U_e\theta/\nu = 13600$ are from data ⊙, $y/\delta = 0{\cdot}4$; ⊡, 0·6; ▽, 0·8. (*a*) $-\overline{u^3}$; (*b*) $\overline{u^2v}$; (*c*) $-\overline{uv^2}$; (*d*) $\overline{v^3}$.

4. Conclusions

The present mean-flow data, and in particular the good agreement between Preston-tube and Stanton-tube measurements of the skin friction (figure 5), indicate that the observed changes in mean-velocity profiles at low Reynolds number arise because of a reduction in the wake component and not through a failure of the inner-layer logarithmic law. This conclusion supports the suggestion of Huffman & Bradshaw (1972) that the main source of low-Reynolds-number effects is the viscous superlayer, which forms the interface between the turbulent and irrotational parts of the flow.

Although the present data do not directly demonstrate the point, it seems very likely that the 'typical-eddy' motions found by Falco (1974), the size of which scale on ν/u_τ rather than on δ, in fact represent the excursions of the viscous superlayer around the nominal outline of the larger eddies.

The question of whether the typical eddy motions arise from Kelvin–Helmholtz instability or some other form of instability of the interface may not be a meaningful one, but the 'typical-eddy' shape observed by Falco and by Head & Bandyopadhyay resembles the inclined horseshoe vortex, which is the normal mode of instability of a spanwise vortex line in a mean shear. Many authors, starting with Theodorsen (1952), have suggested that the horseshoe vortex is the basic large-eddy disturbance in a turbulent shear layer (even the inclined vortex pair of Townsend (1976) can be interpreted as part of a horseshoe vortex) and it is at least *a priori* plausible that any instability mode of the viscous superlayer should be similar to that of the boundary layer as a whole since both are vortex sheets in the large.

Zone-length probability distributions for, say, the turbulent zones depend very strongly on the shortest irrotational interval that is counted as real, and the simplest meaningful way of presenting zone-length data at a single y-position is as a conditional probability map of zone-length p.d.f.s for different values of the shortest zone length that is regarded as significant (e.g. figure 11). Previous workers' use of a simple average zone length are as unrealistic as attempts to describe the broad spectrum of the velocity field in terms of a single frequency. However, modes or moments of the p.d.f.s for a suitable choice of minimum zone lengths do give

meaningful single lengthscales, and our results show conclusively that the ratio of the interface lengthscale to the boundary-layer thickness becomes independent of Reynolds number above $Re_\theta \approx 5000$, where the wake component also becomes constant. Since the superlayer thickness and the 'typical-eddy' size continue to decrease, relative to δ, as Re increases, we conclude that the typical eddies have a negligible effect on the large-scale shape of the interface, and on the Reynolds stress and mean velocity profile, at high Reynolds numbers.

The simpler anisotropy parameters made with the second-order mean products of turbulent fluctuations change rather rapidly with Reynolds number below $Re_\theta = 5000$. $\overline{u^2}/\overline{v^2}$ increases monotonically with Reynolds number while the shear correlation coefficient (figure 28) reaches a weak maximum at $Re_\theta = 2000$ and then decreases to an asymptotic value at high Reynolds numbers. Triple products normalized by the local shear stress, however, rise only slowly with Reynolds number, and the simplest explanation is that the large-eddy structure (or at least the parts of it responsible for turbulent transport) is still present, although somewhat weakened, at low Reynolds number. The Reynolds-number independence of the intermittency profile supports this explanation.

The most noticeable feature of the turbulent energy balances (figure 29) is that the advection (the transport of turbulent energy by the mean velocity) is rather small at low Reynolds numbers; the boundary-layer thickness increases with x but the turbulent energy at given y/δ decreases. As usual, values of dissipation length parameter deduced from measurements of dissipation-by-difference are rather scattered, but they confirm the increase in lengthscale found empirically to be necessary to optimize calculations of turbulent boundary layers at low Reynolds number.

We particularly wish to acknowledge the extensive and penetrating comments of an anonymous referee on a draft of this paper: even where we have not accepted his views they have been of great value in clarifying ours. We are grateful to Dr J. Andreopoulos for access to his high-Reynolds-number data, to Dr I. P. Castro, Dr J. E. Green, the late Professor L. S. G. Kovasznay, Professor J. Laufer, Dr Muck Kin-Choong and Dr D. H. Wood for helpful discussions, and to the Science Research Council for financial support.

REFERENCES

ANDREOPOULOS, J. 1978 Symmetric and asymmetric near wake of a flat plate. Ph.D. thesis, Imperial College, London.

ANDREOPOULOS, J. & BRADSHAW, P. 1980 Measurements of interacting turbulent shear layers in the near wake of a flat plate. *J. Fluid Mech.* **100**, 639.

BATCHELOR, G. K. 1953 *The Theory of Homogeneous Turbulence.* Cambridge University Press.

BRADSHAW, P. 1971 *An Introduction to Turbulence and Its Measurement.* Pergamon.

BRADSHAW, P. 1972 Two more low-turbulence wind tunnels driven by centrifugal blowers. *Imperial College Aero. Rep.* no. 72–10.

BRADSHAW, P. 1974 The effect of mean compression or dilatation on the turbulence structure of supersonic boundary layers. *J. Fluid Mech.* **63**, 449.

BRADSHAW, P. & MURLIS, J. 1974 On the measurement of intermittency in turbulent flows. *Imperial College Aero. Rep.* no. 74–04.

BREDERODE, V. & BRADSHAW, P. 1978 Influence of the side walls on the turbulent centre plane boundary layer in a square duct. *Trans. A.S.M.E.* I: *J. Fluids Engng* **100**, 91.

BROWN, G. L. & THOMAS, A. S. W. 1977 Large structure in a turbulent boundary layer. *Phys. Fluids* **20**, S243.

BUSHNELL, D. M., CARY, A. M. & HOLLEY, B. B. 1975 Mixing length in low Reynolds number compressible turbulent boundary layers. *A.I.A.A. J.* **13**, 1119.

CASTRO, I. P. 1973 A highly distorted turbulent free shear layer. Ph.D. thesis, Imperial College, London.

CASTRO, I. P. & BRADSHAW, P. 1976 The turbulence structure of a highly curved mixing layer. *J. Fluid Mech.* **73**, 265.

CHEN, C. H. P. & BLACKWELDER, R. F. 1978 Large scale motion in a boundary layer: a study using temperature contamination. *J. Fluid Mech.* **89**, 1.

CHEVRAY, R. & TUTU, N. K. 1978 Intermittency and preferential transport of heat in a round jet. *J. Fluid Mech.* **88**, 133.

COLES, D. E. 1962 The turbulent boundary layer in a compressible fluid. *Rand Rep.* R403–PR, ARC 24473: Appendix A: A manual of experimental boundary layer practice for low speed flow.

COLES, D. E. & HIRST, E. A. (Eds.) 1969 *Proc.* 1968 *AFOSR-IFP-Stanford Conf. on computation of turbulent boundary layers.* Thermosciences Division, Stanford University.

CORRSIN, S. & KISTLER, A. L. 1955 Free stream boundaries of turbulent flows. *NACA Rep.* no. 1244.

DEAN, R. B. 1977 A single formula for the complete velocity profile in a turbulent boundary layer. *Trans. A.S.M.E.* I: *J. Fluids Engng* **98**, 723.

DEAN, R. B. & BRADSHAW, P. 1976 Measurements of interacting shear layers in a duct. *J. Fluid Mech.* **78**, 641.

FALCO, R. E. 1974 Some comments on turbulent boundary layer structure inferred from the movements of a passive contaminant. *A.I.A.A. Paper* no. 74–99.

FALCO, R. E. 1977 Coherent motions in the outer region of turbulent boundary layers. *Phys. Fluid Suppl.* **20**, S124.

FALCO, R. E. 1980 Combined simultaneous flow visualization/hot-wire anemometry for the study of turbulent flows. *Trans. A.S.M.E.* I: *J. Fluids Engng* **102**, 174.

FIEDLER, H. (ed.) 1978 *Structure and Mechanisms of Turbulence I, II.* Lecture Notes in Physics, vols. 75, 76. Springer.

FIEDLER, H. & HEAD, M. R. 1966 Intermittency measurements in the turbulent boundary layer. *J. Fluid Mech.* **25**, 719.

FINLEY, P. J., PHOE, K. C. & POH, C. J. 1966 Velocity measurements in a thin turbulent water layer. *Houille Blanche* **21**, 713.

GRANT, H. L. 1958 The large eddies of turbulent motion *J. Fluid Mech.* **4**, 149.

GREEN, J. E. 1971 A note on the turbulent boundary layer at low Reynolds number in compressible flow at constant pressure. Personal communication.

HANCOCK, P. E. 1980 The effects of free stream turbulence on turbulent boundary layers. Ph.D. thesis, Imperial College, London.

HEAD, M. B. & BANDYOPADHYAY, P. 1981 New aspects of turbulent boundary-layer structures. *J. Fluid Mech.* **107**, 297.

HEDLEY, T. B. & KEFFER, J. F. 1974*a* Turbulent/non-turbulent decisions in an intermittent flow. *J. Fluid Mech.* **64**, 675.

HEDLEY, T. B. & KEFFER, J. F. 1974*b* Some turbulent/non-turbulent properties of an intermittent flow. *J. Fluid Mech.* **64**, 645.

HUFFMAN, G. D. & BRADSHAW, P. 1972 A note on von Kármán's constant in low Reynolds number turbulent flows. *J. Fluid Mech.* **53**, 45.

INMAN, P. N. & BRADSHAW, P. 1981 Mixing length in low Reynolds number, low speed turbulent boundary layers. *A.I.A.A. J.* **19**, 653.

KLEBANOFF, P. S. 1955 Characteristics of turbulence in a boundary layer with zero pressure gradient. *NACA Rep.* no. 1247.

KLINE, S. J. & FALCO, R. E. 1980 Summary of the AFOSR/MSU Research Specialists Workshop on Coherent Structure in Turbulent Boundary Layers. *AFOSR* TR-80-0290.

KOVASZNAY, L. S. G., KIBENS, V. & BLACKWELDER, R. F. 1970 Large scale motions in the intermittent region of a turbulent boundary layer. *J. Fluid Mech.* **41**, 283.

LARUE, J. C. & LIBBY, P. A. 1974 Temperature fluctuations in the plane turbulent wake. *Phys. Fluids* **17**, 1956.

MABEY, D. G. 1977 Some observations on the wake component of the velocity profiles of turbulent boundary layers at subsonic and supersonic speeds. *RAE Tech. Rep.* TR 77004.

MABEY, D. G. 1979 *Aero. Q.* **30**, 590.

MUCK, K. C. 1980 Comparison of various schemes for the generation of the turbulent intermittency function. *Imperial College Aero. Rep.* no. 80–03.

MURLIS, J. 1975 The structure of a turbulent boundary layer at low Reynolds number. Ph.D. thesis, Imperial College, London.

PAIZIS, S. T. & SCHWARTZ, W. H. 1974 An investigation of the topography and motion of the turbulent interface. *J. Fluid Mech.* **63**, 315.

PATEL, V. C. 1965 Calibration of the Preston tube and limitations on it use in pressure gradients. *J. Fluid Mech.* **23**, 185.

PRESTON, J. H. 1958 The minimum Reynolds number for a turbulent boundary layer and the selection of a transition device. *J. Fluid Mech.* **3**, 373.

PURTELL, L. P., KLEBANOFF, P. S. & BUCKLEY, F. T. 1981 Turbulent boundary layers at low Reynolds numbers. *Phys. Fluids* **24**, 802.

SANDBORN, V. A. 1959 Measurements of intermittency of turbulent motion in a boundary layer. *J. Fluid Mech.* **6**, 221.

SIMPSON, R. L. 1970 Characteristics of turbulent boundary layers at low Reynolds numbers with and without transpiration. *J. Fluid Mech.* **42**, 769.

SMITH, C. R. & ABBOTT, D. E. (eds.) 1978 *Coherent Structure of Turbulent Boundary Layers: Proc. AFOSR/Lehigh University Workshop.* Mech. Engng Dept. Lehigh University.

THEODORSEN, T. 1952 Mechanism of turbulence. In *Proc. 2nd Midwestern Conference on Fluid Mechanics, Ohio State University*, p. 1.

TOWNSEND, A. A. 1956 *The Structure of Turbulent Shear Flow.* Cambridge University Press.

TOWNSEND, A. A. 1976 *The Structure of Turbulent Shear Flow*, 2nd edn. Cambridge University Press.

WEIR, A. D. & BRADSHAW, P. 1974 Apparatus and programs for digital analysis of fluctuating quantities in turbulent flow. *Imperial College Aero. Rep.* no. 74–09.

WEIR, A. D., WOOD, D. H. & BRADSHAW, P. 1981 Interacting turbulent shear layers in a plane jet. *J. Fluid Mech.* **107**, 237.

WIEGHARDT, K. 1944 Zum Reibungswiderstand rauher Platten. *Kaiser-Wilhelm-Institut für Strömungsforschung, Göttingen*, UM 6612.

WILLMARTH, W. W. 1975 Structure of turbulence in boundary layers. *Adv. Appl. Mech.* **15**, 159.